30

8153 6

ADVANCED HIGH-FREQUENCY ELECTRONIC BALLASTING FOR GAS DISCHARGE LAMPS

by

ZAKI MOUSSAOUI
M.S. University of Central Florida, 1994

A dissertation submitted in partial fulfillment of the
requirements
for the degree of Doctor of Philosophy
in the School of Electrical Engineering and Computer Science
in the College of Engineering and Computer Science
at the University of Central Florida
Orlando, Florida

Spring Term
2003

Major Professor: Dr. Issa Batarseh

Disclaimer: Potential users of the methods and schematics described in this dissertation are advised that such use could potentially violate patent rights of one or more third parties. Author disclaims any liability, which may arise from applying the methods and schematics that users should consult their own legal advisors.

ABSTRACT

Electronic ballasts for arc discharge lamps are becoming more and more popular because of their small size, light weight, high efficacy, longer lifetime and controllable output. However, power line quality efficiency, electromagnetic interference (EMI) and cost are issues that have to be considered when choosing a ballast.

This dissertation addresses advanced high-frequency electronic ballasting technique using a single switch to achieve a high power factor correction, zero voltage switching, and a good dimming performance. The proposed topology will be shown to achieve up to 89 percent efficiency due to the zero-voltage switching. Using the input voltage as duty cycle modulator, near 98 percent power-factor correction is attainable. Utilizing the frequency control capability of the class E converter and the frequency control technique of a resonant converter, a 10 percent dimming down capability is possible.

Size and cost reduction is achieved owing to the use of a single inductor as the storage element for the boost side and for power delivery, and a single switch for power delivery. Due to the interaction between the PFC stage and the inverter stage, extremely high bus-voltage stress may exist during the dimming operation. To reduce the bus voltage and achieve a wide-range dimming control, a novel voltage clamping method is proposed to increase the power factor correction and reduce the stress on the switching component.

Experimental results show that a wide, stable dimming operation is achieved with constant switching frequency and variable duty cycle or a combination of both.

ACKNOWLEDGEMENTS

I would like to express my sincere appreciation and gratitude to my advisor, Dr. Issa Batarseh, for his guidance and support throughout the course of this work. His extensive knowledge, creative thinking and rigorous research attitude have guided me through the research and made this work possible.

I would also like to thank my doctoral committee members, Christopher J. Iannello, Takis C. Kasparis, Wasfy B. Mikhael, and Kalpathy B. Sundaram for their helpful suggestions. Thanks also go to the Florida PEC team and staff for their countless support.

Special thanks goes to my Brother Khalid and his family for their help, support and encouragement. My wife Ghita for her love, understanding, and support during the past years and my lovely son, Mehdi, who gave me the utmost joy of being a father.

Finally, I would like to give my heartfelt appreciation to my parents, Ahmed and Khadija who brought me up with their love and encouraged me to pursue further education.

TABLE OF CONTENTS

LIST OF TABLES

LIST OF FIGURES

CHAPTER 1

INTRODUCTION

Light and light sources have always played an important role in our day-to-day living. Man always tried to conquer his fear of darkness by creating light. Light is defined as visually evaluated radiant energy, which stimulates man's eyes and enables him to see [A1]. The first type of light source used was combustion [A4] followed by incandescence type, which is the radiation emitted by a hot body [A4-A5]. Since its introduction, the incandescent lamp has been very popular because of its ease of production and low price. The third major type of light source is the arc discharge lamp. Through the Nineteenth Century, the development of arc discharge and incandescent lamps proceeded side by side [A4-A6]. In the late 19^{th} century, the gas discharge lamp became more and more popular because of its high efficiency, and long life expectancy. Today, there are more than 6,000 types of light bulbs being manufactured, most of which can be placed in the following six categories: incandescent, tungsten, halogen, fluorescent, mercury, metal halide, and sodium [A4-A6]. Table 1.1 shows a comparison of several types of lamps with their performance characteristics.

Table 1-1 Comparison of Various Lamp Characteristics

Lamp Type	Lamp efficiency (lm/W)	Life (h)	% Lumen/ Depreciation	Color rendering
Incandescent	9-22	750- 2,500	10-12	100
Fluorescent	45-95	7,500-20,000	11-28	80-60
Metal Halide	80-115	7,500-15,000	13-22	60-40
High-Pressure S	80-140	12,000-24,000	8-10	40-20

The major characteristics to be considered when choosing a lamp are its luminous efficacy, life, lumen depreciation, and color rendering [A1]. Luminous efficacy is the measure of the lamp's ability to convert the electric input power in watts into output luminous flux in lumens. It is measured in lumens (lm) per watt (lm/W)[A7]. The luminous flux of a light source is the electromagnetic radiation within the visible part of the electromagnetic spectrum multiplied by the sensitivity of man's eye to that part of the light emitted from the source (Figure1-1). The visible portion of the spectrum covers the wavelength range from approximately 380 nm to 780 nm as shown in Fig. 1-2 (a). The eye discriminates between different wavelengths in this range by the sensation of color in the manner illustrated by Fig. 1-2b [A7,A8].

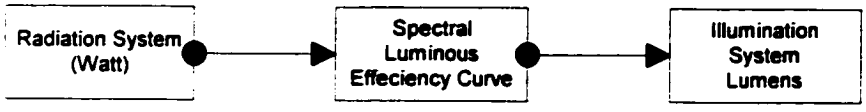

Figure 1-1. Relating Watts to Lumens

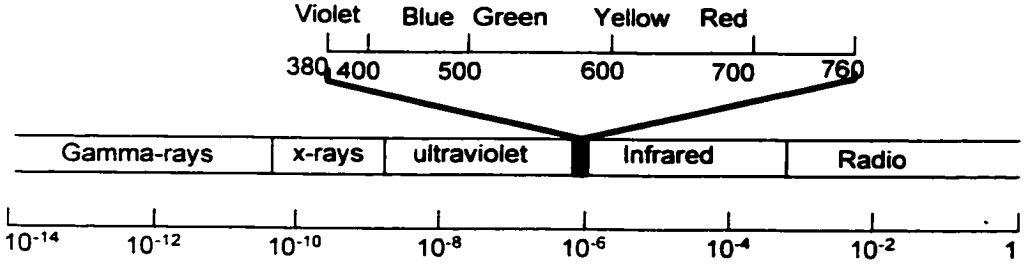

Figure 1-2a. The Electromagnetic Spectrum

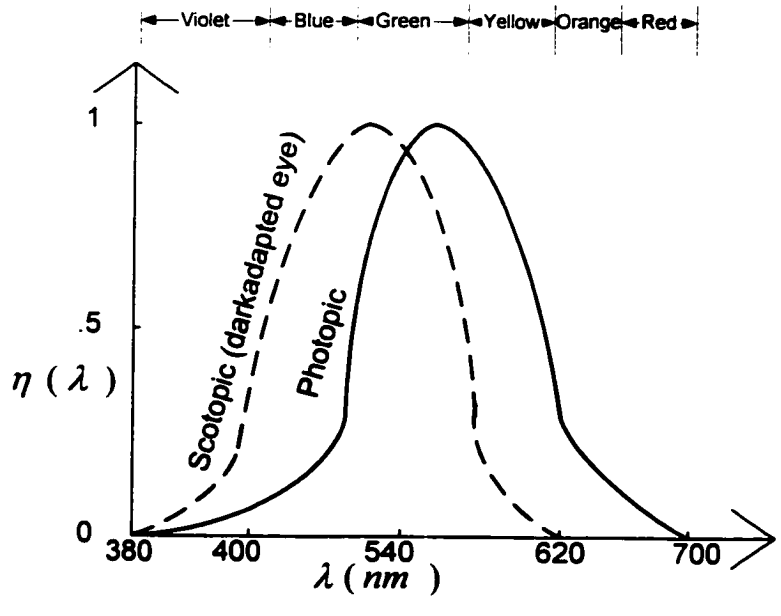

Figure 1-2b. Spectral Luminous Efficiency Curves

The life of a lamp is the number of hours it takes for approximately 50 percent of a large group of lamps of the same kind to fail. Failure means that the lamp will no longer light or that light output has dropped to a specific percentage value. Finally, there is the matter of color rendering. The lamp types do not provide the same nominal "white." Their difference in spectral distribution can produce two effects within a lighted space. Some of the colors of objects within that space can appear unnatural or faded – reds can appear brown, violets nearly black, etc. Second, the entire space may "feel" warm or cool. For example, a mercury lamp, lacking in reds and oranges, makes a space seem cool, whereas an incandescent lamp, with deficiencies in the blue and violets, makes a space feel warm. From the above discussion and using Table 1-1, we can see that gas discharge lamps have a better performance than incandescent lamps. One of the major reasons why incandescent lamps still exists in the market is their low price. While incandescent lamps can be connected directly to any suitable power supply, all gas discharge lamps require a suitable circuit and control gear or a ballast component for starting and operation.

1.1 Ballast Requirement

The ballast has to perform four functions: provide start up voltage, maintain constant current, stabilize the circuit-under-fault, and comply with the applicable requirement of regulation. Every gas discharge lamp requires higher-than-normal voltage to initiate the ionization process, as shown in Fig. 1-3. The voltage required for lamp starting depends on the size and mixture of gas in the tube, the temperature, humidity, and any electrical fields [A5]. There are many techniques used to control and guarantee the starting voltage

of the lamp: preheating of the cathodes, superimposed high voltage pulses, and an auxiliary starting electrode inside the lamp.

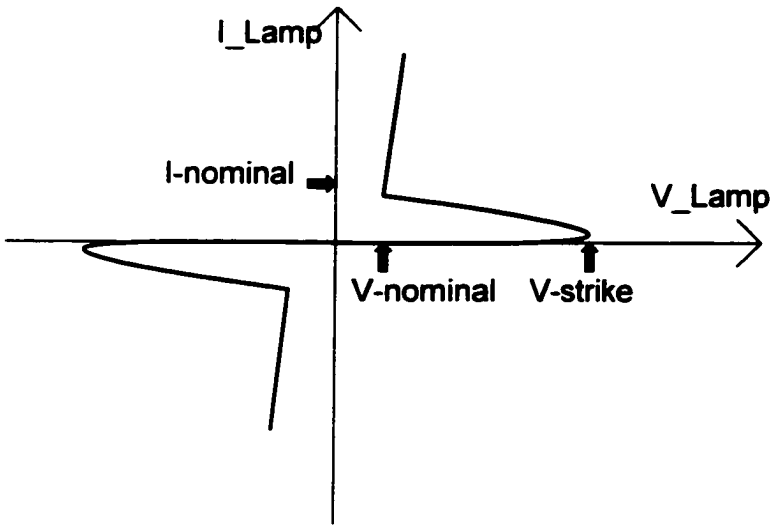

Figure 1-3 Typical Low Pressure Fluorescent Tube I/V Characteristics

As can be seen from Fig. 1-3, the relationship between the voltage cross and the current through the lamp in the arc discharge region has a negative slope; it is in this region that most lamps operate. To prevent current runway from a constant voltage source, a ballast system is used. Another necessary requirement for the proper operation of the lamp is the use of an alternative power source.

A simple ballast system that can meet this requirement could be a series resistor, but it is very inefficient. The most common ballast system used in the market today is the magnetic ballast. It consists of an inductor for current limitation and bi-directional switch for lamp arcing as shown in Fig 1-4. Although magnetic ballasts have the advantages of

low cost and high reliability, there exists many performance limitations due to the low-frequency operation in 50/60Hz line frequency. The fact that the gas ionization time constant is around 1ms, reigniting the lamp every half cycle is necessary. This reignition results in non-sinusoidal waveforms of voltage and current cross the load, and an increase of harmonics in the system.

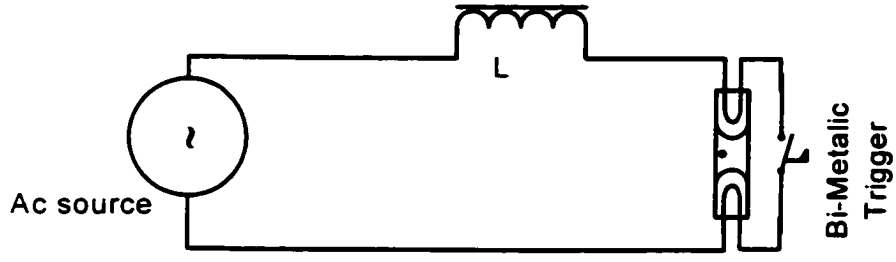

Figure 1-4. Standard Ballast Circuit for Fluorescent Tube

After every line-zero crossing, the lamp voltage waveform has a restrike voltage peak; during the rest of the cycle, the voltage does not vary much. This causes two major problems: The lamp electrode wearing is significant, and lamplight output is highly susceptible to the line voltage and is modulated by the line frequency. This light modulation can cause discomfort and also what is known as "sick building syndrome" [F6]. The weight and volume of the inductor is large in order to support the 50/60 Hz operations. Finally, there is no efficient and cost-effective way to regulate the lamp power. These drawbacks led to the use of high-frequency AC current to drive the discharge lamps. High-frequency operation not only results in significant ballast volume

and weight reduction, but also improves the gas discharge lamp property. In the case of fluorescent lamps, as the frequency increases beyond about 1kHz the ionization state can no longer follow the rapid change of lamp current, which results in near-constant plasma density and almost constant effective impedance, as shown in Fig. 1-5. The operation of the lamp at high frequency reduces the electrode losses and the overall lamp efficiency is improved, as shown in Fig. 1-6.

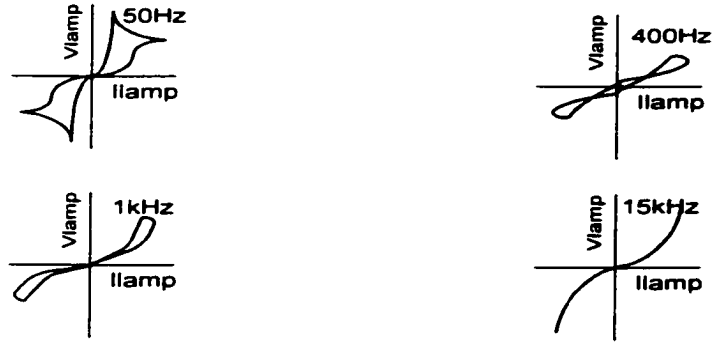

Figure 1-5 Dynamic Volt-Ampere Characteristics of a Fluorescent Lamp Operated at Various Frequencies

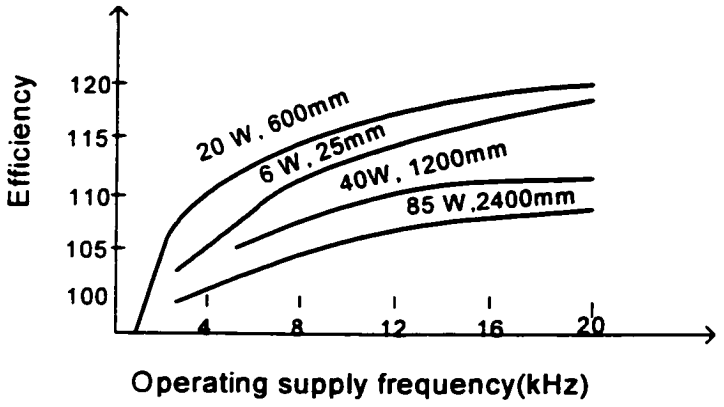

Figure 1-6. Lamp Efficiency (lm/W) at Various Frequencies of the Operation Voltage

1.2 Dissertation Outline

Chapter 1 introduces the research background and literature reviews, and it provides the research objectives and outline. Chapter 2 offers a literature overview of the existing ballasts, and highlights the single-stage boost-derived power factor corrector techniques. Also in Chapter 2, the motivation and the objective behind the proposed research will be given. Chapter 3 will show the proposed single-stage zero-voltage-switching (ZVS) ballast circuit synthesis. Chapter 3 will also give a detailed analysis and generalized circuit equation for optimization and design. Circuit simulation and experimental results will be given and evaluated. In Chapter 4 the draw back of the proposed circuit of Chapter 3 will be discussed, and a set of proposed solutions will be analyzed. The simulation and experimental results of the new proposed topology will be given in Chapter 4. Dimming capabilities of the proposed topology will be verified and analyzed.

Chapter 5 summarizes the major results of the work and offers suggestions for future work.

CHAPTER 2

BALLAST EVOLUTION AND COMPARISON

2.1 Ballast Classification

Electronic ballasts are essentially power inverter circuits that change the input line current and frequency in order to supply the lamp with an energy source that meets its requirement. The ballast also has to perform a number of additional functions, including starting the lamp, maintaining a running current at the designed value, controlling and protecting the load in case of over voltage or lamp failure, and meeting any of the agency's regulation and safety requirements. The ballast can be classified as double-switch or single-switch schemes [B1]. The double-switch can be divided into two main categories, push-pull or half bridge, as shown in Figs. 2-1 and 2-2, respectively.

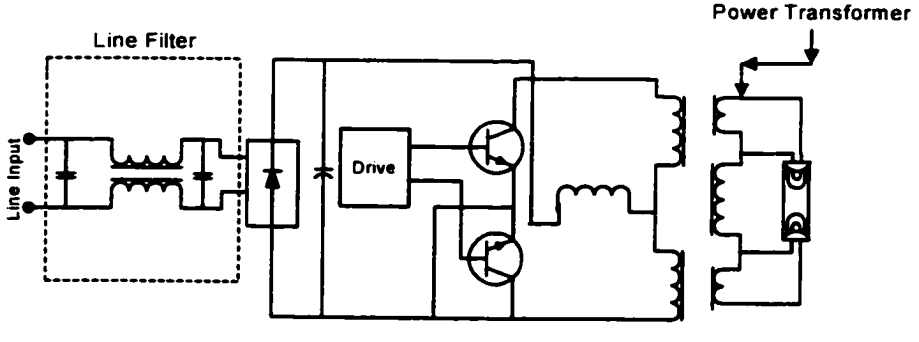

Figure 2-1. Typical Current Fed Push–Pull Converter

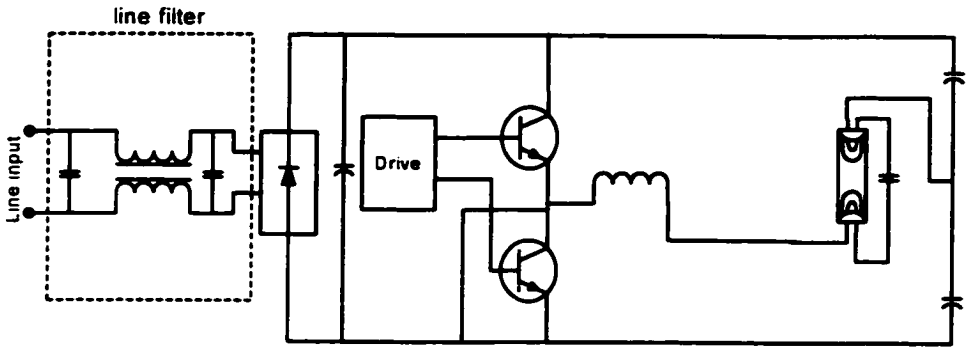

Figure 2-2. Typical Half Bridge Topology

The half-bridge is, by far, the most widely used in Europe (100% of the so–called Energy Saving Lamps and Industrial applications are based on this topology), while the push–pull is the preferred solution in the USA, with around 80% of the electronic lamp ballasts using this scheme today [B1]. Both of these topologies have their advantages and drawbacks, as shown by Table 2-1 [B1, B2]. The main advantage of the current fed push–pull converter, besides the common grounded-emitter structure, is the ruggedness of this topology since it can sustain a short circuit of the load without any damage to the power switches (assuming they were sized to cope with the level of current and voltage generated during such a fault condition). This is a direct benefit of the current mode brought by the inductor in a series with the VAC line.

Table 2-1. Main Characteristics of the Dual Switches Topologies

Parameters	Half Bridge Topology	Push–Pull Topology
V (BR)CER	700 V*	1100 V - 1600 V*
Inrush Current	3 to 4 times I nom **	2-3 times I nom **
t si window	2.60 ms–3.60 ms	1.90 – 2.30 ms
Drive	High & Low side	Low side only

Notes: *numbers are typical for operation on a 230 V line.
Notes: ** I nom: current into the transistors in steady state.

However. the imbalance in both the power transistors and the magnetic circuit leads to high voltage spikes that make this topology difficult to use for line voltage above 120 V, or if the front is connected to the typical 400 volts of a power-factor corrected source. Additionally, the dimming function became practically very difficult because of the needed additional symmetry control in order not to saturate the transformer. On the other hand, a half-bridge does not impose a high stress on the switches and also does not suffer from the difficulty in dimming.

2.2 The Half-Bridge Resonant Topology

As was mentioned earlier, the half bridge resonant topology is the most commonly used ballast circuit in the market. There are three major half-bridge circuits given in Figs. 2-3, 2-4. 2-5. They are classified according to their Crest Factor (CF) and Power Factor (PF) characteristics.

2.2.1 Crest Factor.

In high-frequency operation, a low lamp current Crest Factor is preferred. The Crest Factor (CF) is defined as the ratio of the peak to the root-mean-square (RMS) current value, given by Eq. (2-1).

$$CF = \frac{I_{peak}}{I_{rms}} \qquad (2\text{-}1)$$

The CF plays a significant role in ballast performance. As studies show, the electrode life is very sensitive to the CF, and the life of a gas discharge lamp is basically determined by its electrode's life. The higher the CF, the shorter is the lamp life. A pure sine wave without modulation has a CF of $\sqrt{2}$, a triangular wave has a CF of 1.7. American National Standards Institute (ANSI) specifications recommend that the maximum CF be 1.7 [B3]. The lamp life will drop to less than half if the CF becomes 2 [A11]. The CF is also a matter of lamplight flickering. Unlike in low frequency magnetic ballasts where the flickering is caused by the jitter of the ignition angle in a half-line cycle, the flickering in a high frequency ballast is caused by the use of a modulated drive current to the lamp and the zero current into the lamp every half input cycle. To maintain a low CF, a low AC component input voltage is necessary to handle the variations between the input pulsating

power and the constant output lamp power. A conventional practice is to locate a bulk capacitor right behind the diode rectifier, as shown in Fig. 2-4. This is a rather simple solution to improving CF, if the Power Factor is not an issue. The above mentioned solution for the CF draws current from the AC line in only a small conduction angle as shown in Fig. 2-4, producing a very poor power factor with rich harmonic currents that cause many known undesirable effects.

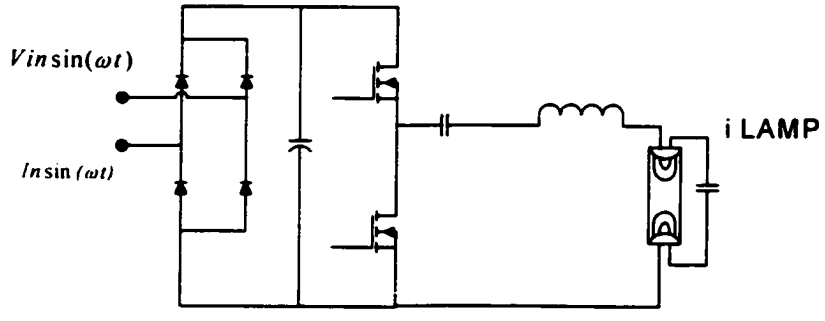

Figure 2-3 Series Resonant Half-Bridge with Low Harmonics and High Crest Factor

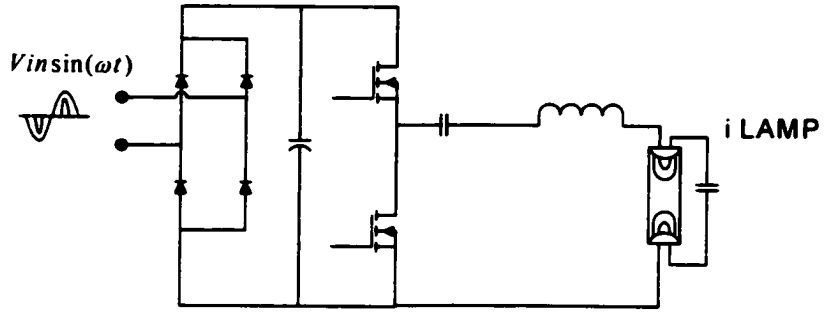

Figure 2-4 Series Resonant Half -Bridge with High Harmonics and Low Crest Factor

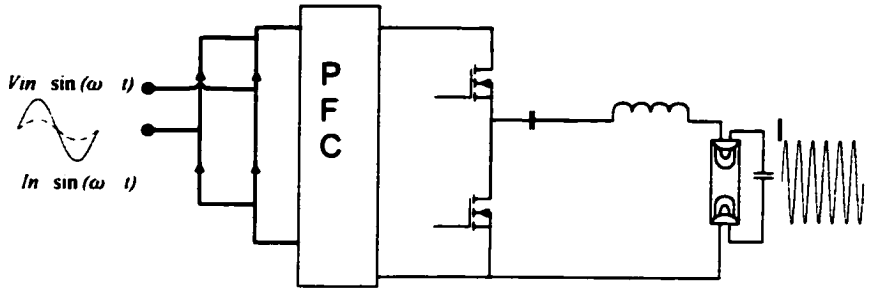

Figure 2-5 Series Resonant Half -Bridge with Low Harmonics and Low Crest Factor

2.2.2 Power Factor Corrector and Total Harmonics Distortion

The harmonics disturbance became an issue that needed to be dealt with in mid 60s, when the electromagnetic interference (EMI) affected the communications system [B4-B5]. Now, with the increased use of high power semiconductors and high frequency switching components in energy conversion, loads with nonlinear characteristics such as ballasts have gradually constituted the major portion of electrical loads in most of the power systems. This issue became problematic and affected every system connected to the grid. Most of the electrical equipment has been designed and manufactured to operate efficiently assuming an ideal sinusoidal environment. In a polluted system, however, their operation may be deviated from the designed normal operation or may operate under stress conditions. It was shown that power system harmonics are found to be the major threat to the safe operation of the power systems. Some of their influences are: excessive heating in transformers and motors by increasing magnetic core losses, abnormal audible noises and mechanical vibration of the transformers and motors, malfunction of

protection relays, accelerate aging of insulating media, increased instrument error, overloading of shunt capacitor banks [B15-B17]

In view of the proliferation of the power electronic equipment connected to the utility grid, some national and international harmonic standards have been developed to limit harmonic current injection or to limit the harmonic voltages at the point of common coupling (PCC) [B8-B10] to protect power system safety operation. The major one that governs the lighting industry is IEC 1000 Family. The underlined consideration of the standard is to prevent harmonic currents generated by nonlinear loads from interfering with other customers. In other words, the electric utility and the user of electrical equipment are both responsible for improving the power quality. IEC 1000-3-2 classifies power electronics equipment with a maximum input current less than or equal to 16A per phase into four categories. Among those, the harmonic limits of the class C received the most attention in the lighting industry. Table 2-2 shows the harmonic current limits of this class.

Table 2-2. IEC 1000-3-2 Harmonic Current Limits For Class C Electrical Equipment

Harmonic order, n	Maximum permissible harmonic current per watt, mA/W	Maximum permissible harmonic current, A
3	3.4	2.30
5	1.9	1.14
7	1.0	0.77
9	0.5	0.4
11	0.35	0.33
13≤n≤39, odd harmonics	3.85/n	Refer to class A

Other than the PFC, another important measure of the input-current quality is the total harmonic distortions (THD), defined in Eq. (2-1) where I_k is the RMS value of the k_{th} current harmonic. The relationship between PFC and THD can be expressed in Eq. (2-2), where there is no DC component in the input current.

$$PF = \frac{Averagepower}{Aparentpower} = \frac{I_1}{I_{rms}}\cos(\theta)$$

$$THD = \sqrt{\frac{\sum_{i=2}^{\infty} I_i^2}{I_1^2}} \qquad (2\text{-}2)$$

$$PF = \frac{\cos\theta}{\sqrt{1+THD^2}} \qquad (2\text{-}3)$$

To achieve high PF and low current harmonics, the use of a power factor (PF) correction or input-current-shaping (ICS) method is necessary. One simple approach is to use a passive filter. However, passive filter components are usually bulky and ineffective. A more effective approach is to use active means. A common practice is to employ the so called two-stage approach, in which a switching mode PFC stage is added to the conventional electronic ballast, providing almost unity PF. AC/DC rectification from the utility line, as shown in Fig. 2-5.

2.3 Single-Stage Power Factor Correction Inverter

2.3.1 Generalized Power Factor Techniques

In the past several years, many topologies and control approaches were presented in the active power-factor corrector area. Depending on the topology, active PFC converters can be divided into categories. First we have the two-stage PFC converter, which consists of a PFC stage and a DC/DC conversion stage. The PFC stage will convert utility-line voltage

to a constant DC voltage with a high power factor. The DC/AC conversion stage will convert that constant DC voltage into the required AC voltage necessary for the specific lamp. Those two stages can be optimally designed since they operate independently. This approach is economically feasible in high power applications like high-pressure sodium and HID lamps above 250W. The scheme and typical topology are shown in Fig. 2-6; its advantages include superior performance and flexible design configuration, but its cost is high due to its complex configuration.

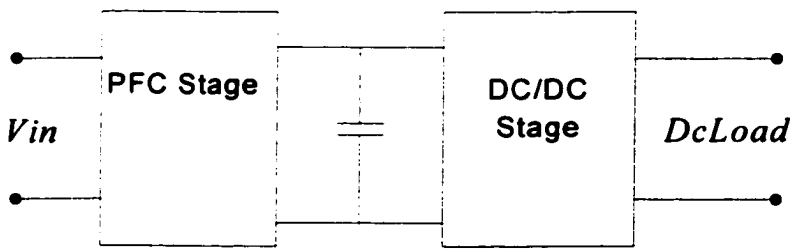

Figure 2-6 Two-Stage PFC Converter Structure

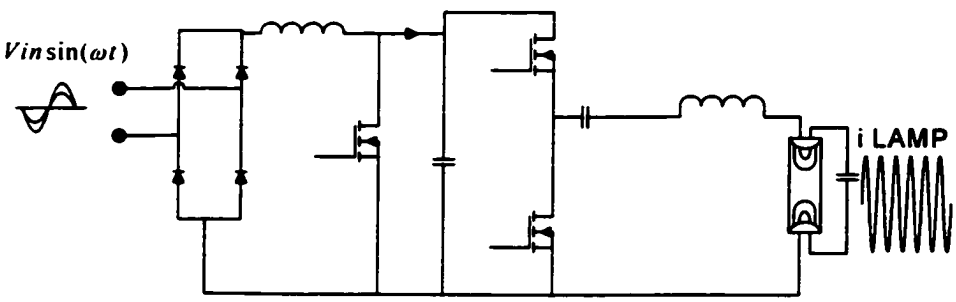

Figure 2-7 Typical Half -Bridge Two-Stage PFC Converter

Second, we have the single-stage PFC converter: The PFC stage and DC-AC conversion stage in this approach are integrated into one stage with a single controller and shared

active switches. Normally the controller is designed only to achieve tight output power, while high power factor is achieved by specified topologies with automatic waveform shaping function, such as boost topology with constant duty-cycle control. A single stage PFC converter is more attractive for low power applications because of its simple configuration and low cost. So many single-stage PFC circuits were proposed and analyzed in the literature. Based on these original single-stage PFC techniques, numerous modified circuits were discussed in articles and patents [B-22, B-35].

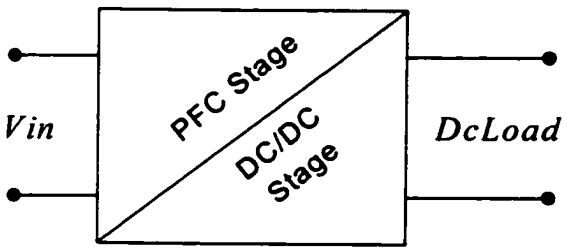

(a). Typical Configuration

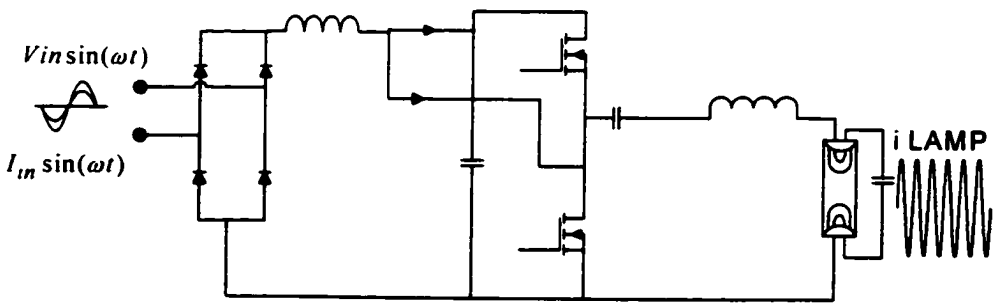

(b). Typical Topology

Figure 2-8 Single-Stage PFC Converter: (a) Simplified Diagram, (b) Circuit Topology.

From the control aspect of the power system, combining the two stages implies loss of a degree of control. In order to still control the output power and achieve high power factor correction, many techniques are used. According to the conduction mode of the PFC stage, the PFC circuit is categorized as Continuous Conduction Mode (CCM), Discontinuous Conduction Mode (DCM), or Boundary Conduction Mode (BCM). CCM is typically used in high power two stage PFC converters, since its current stress on active switches is the lowest. With specified design of IC chips, very high power factor can be easily achieved. The CCM is mostly used with a two stage approach even though operation can also be implemented to the single stage PFC circuit as mentioned in [B18], but its configuration and control method is too complicated and cost is too high. In DCM, the current in the input inductor goes to zero every switching cycle. This method is commonly used in the single stage PFC converter, since it is easy to get high power factor for some topologies when constant turn-on time control is implemented, even though the current stress on the active switch is much higher than its counterpart at CCM. The DCM due to its simplicity and low cost is still being use in many applications. Finally, there is the Boundary conduction mode. The PFC stage runs at the boundary between the continuous and discontinuous mode, i.e. the new switching cycle begins once the line current reaches zero. With few components and simple control IC, this approach can get high performance without the diode reverse recovery trouble existing in CCM. This approach provides a good tradeoff between high performances and low cost, so it is common in ballast application.

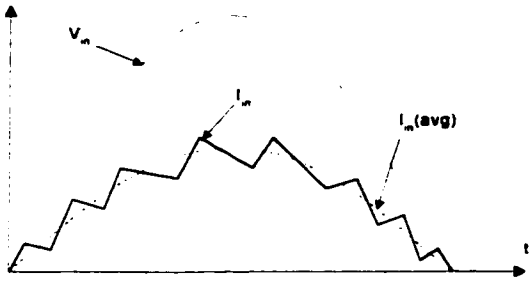

(a) CCM

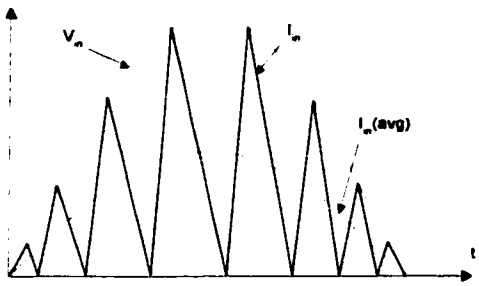

(b) DCM

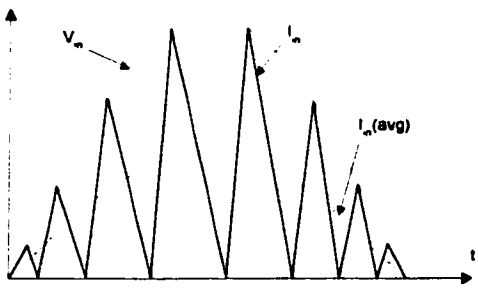

(c) Boundary Mode

Figure 2-9 Current Waveform Under Different Modes of Operation

2.3.2 Transition Mode Power Factor Technique.

To achieve high PFC in DCM the voltage follower approach is used in the control as shown in Fig. 2-10. The operation of the control is straightforward. First an output

reference voltage v_{ref} is achieved by the output feedback. This reference will not change through a complete half input line cycle. This reference voltage v_{ref} will be multiplied by the signal from the input voltage line.

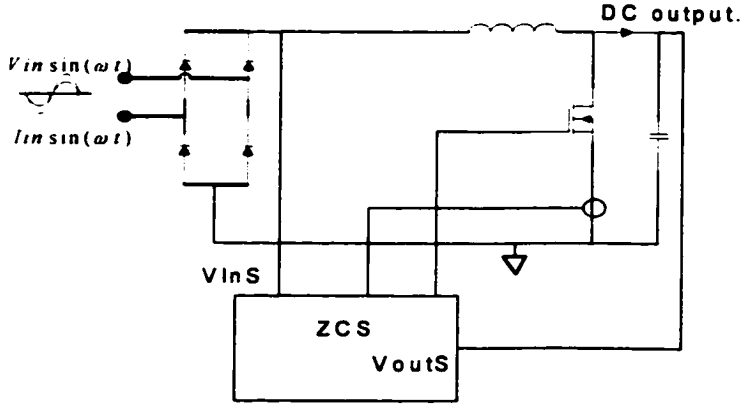

Figure 2-10 Functionality Block Diagram

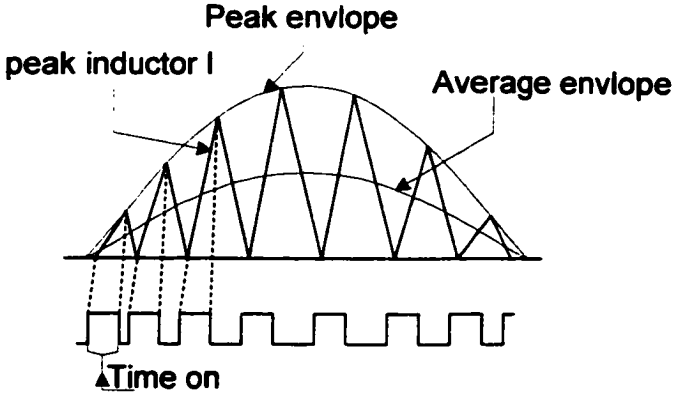

Figure 2-11 Inductor Current and MOSFET Gate Voltage Waveforms

The results of that multiplication dictate the peak current information that guarantee a fixed time-on through a complete half-line cycle.

$$I_{peak} = \frac{V_{in} T_{on}}{L} = \frac{V_m DT}{L} \sin(\omega t) \qquad (2\text{-}3)$$

Where,

$V_{in} = V_m \sin(\omega t)$ is the input voltage, T_{on} is the time on of the switch, and T is the switching period.

$D = T_{on}/T \qquad (2\text{-}4)$

When the switch is turned off, the inductor will discharge to zero in:

$$T_{off} = \frac{I_{PK} \times L}{(V_{out} - V_{In})} \qquad (2\text{-}5)$$

Using Eq. 2.3 we obtain:

The presence of the input filter makes the AC line see an averaged current wave form as shown in Fig. 2-11.

$$I_{in} = I_{on(ave)} + I_{off(ave)} \qquad (2\text{-}6)$$

where, $I_{on(ave)}$ and $I_{off(ave)}$ are the on and off average inductor current.

$$I_{on(ave)} = \frac{V_{in} D^2 T}{2L} \qquad (2\text{-}7)$$

$$I_{off(ave)} = \frac{V_{in}{}^2 D^2 T}{2L(V_{out} - V_{in})} \qquad (2\text{-}8)$$

Using (2-6) (2-8) and after simplification we obtain:

$$I_{in(ave)} = \frac{Vm.\sin(\omega t).V_o.D^2.T}{2.L.(V_{out} - V_{in})} \tag{2-9}$$

Using $\zeta \equiv \frac{D^2 T.V_o}{2.L}$ and $\alpha \equiv \frac{V_m}{V_{out}}$

$$I_{in} = \zeta \frac{\alpha \sin(\omega t)}{1-\alpha \sin(\omega t)} \tag{2-10}$$

As can be seen from Eq. (2.10), as α go to zero the input current approaches sin wave.

From Eq. 2.1:

$$P_{in} = \frac{1}{\pi} \int_0^{\pi} V_{in} I_{in} d\theta \tag{2-11}$$

where,

$$\psi = \int_0^{\pi} \frac{\sin(\theta)^2}{1-\alpha \sin(\theta)}$$

$$\psi := -\frac{-\pi + \sqrt{1-\alpha^2}\,\pi - 2\tan^{-1}\left(\frac{\alpha}{\sqrt{1-\alpha^2}}\right) + 2\alpha\sqrt{1-\alpha^2}}{\alpha^2\sqrt{1-\alpha^2}} \tag{2-12}$$

The input RMS current:

$$i_{rms} = \sqrt{\frac{1}{\pi}\int_0^{\pi} I_{in}^2 d\theta}$$

$$= \zeta\alpha\sqrt{\frac{\Phi}{\pi}}$$

where,

$$\Phi = \int_0^{\pi}\left[\frac{\sin(\theta)}{1-\alpha\sin(\theta)}\right]^2 d\theta$$

$$\phi = \frac{\pi + \sqrt{1-\alpha^2}\,\pi\alpha^2 - \sqrt{1-\alpha^2}\,\pi - 2\pi\alpha^2 + 2\arctan\left(\frac{\alpha}{\sqrt{1-\alpha^2}}\right) - 4\arctan\left(\frac{\alpha}{\sqrt{1-\alpha^2}}\right)\alpha^2 - 2\alpha\sqrt{1-\alpha^2}}{\left(-1+\alpha^2\right)\alpha^2\sqrt{1-\alpha^2}}$$

The power was defined as: $PF = \frac{P_{in}}{V_{rms} \times I_{rms}}$

$$PFC(\alpha) = -\frac{\sqrt{2}\left(-\pi + \sqrt{1-\alpha^2}\,\pi - 2\arctan\left(\frac{\alpha}{\sqrt{1-\alpha^2}}\right) + 2\alpha\sqrt{1-\alpha^2}\right)}{\sqrt{\pi}\,\alpha^2\sqrt{1-\alpha^2}\sqrt{\frac{\pi + \sqrt{1-\alpha^2}\,\pi\alpha^2 - \sqrt{1-\alpha^2}\,\pi - 2\pi\alpha^2 + 2\arctan\left(\frac{\alpha}{\sqrt{1-\alpha^2}}\right) - 4\arctan\left(\frac{\alpha}{\sqrt{1-\alpha^2}}\right)\alpha^2 - 2\alpha\sqrt{1-\alpha^2}}{(-1+\alpha^2)\,\alpha^2\sqrt{1-\alpha^2}}}}$$

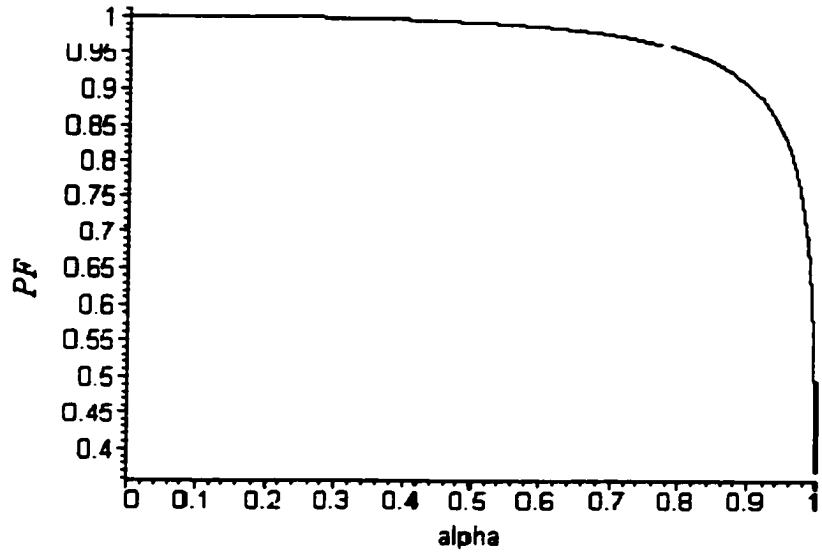

Figure 2-12 Power Factor Correction as Function of α

As can be seen from Fig. 2-12, the PFC will still meet the 93 percent required for ballast application up to $\alpha = 0.8$..

2.4 Dimming Control

Dimming of fluorescent lamps is gaining more and more interest recently. Most of today's dimming control methods can be placed into four categories: variable frequency control, PWM, PFC-stage voltage control, and any combinations of these three. The variable frequency control is the most common in practical implementation because of its simplicity [B37-B43]. As the switching frequency is varied far from the resonant frequency of the tank, the energy transfer to the lamp decreases [B37-B39]. The analytical and experimental studies done by [B37-B39], using this method, show that the

lamp goes into an unstable mode. It either begins to flicker, or they turn off and remain off when dimmed below 30 percent. In general, the dimming of electronic ballasts with frequency control provides only a limited dimming range, typically 3:1. On the other hand, the stable dimming range could be extended by using a DC-link voltage control [B38-B39]. It was shown in [B42] that by selecting a switching frequency close to the natural frequency, the electronic ballasts are seen as current sources controlled by the bus voltage. Flicker-free operation can be maintained when the lamp power is reduced to a small value. However, the lamps tend to show striation as the lamp power drops to a certain level [B42]. In practice, the DC-link voltage control is only used with a variable bus voltage source. Duty-ratio control can achieve a level of performance similar to that of DC-link voltage control, but with a simpler structure. In the asymmetrical duty-ratio control, a small DC-biased lamp current is formed naturally, which helps to prevent the development of striations [B40-B44-B46], although it might cause mercury migration and shorten cathode life.

Good performance could be achieved by combining several control methods. A variable duty ratio and frequency control in a single-stage PFC electronic dimming ballast with a 3:1 dimming range was reported in [B43]. A variable bus voltage and switching frequency control for multiple fluorescent lamp applications in two-stage PFC electronic dimming ballasts with a dimming range of 3:1 has also been introduced [B48]. Another method that was reported is to introduce a dither function into the control to create a non-fixed velocity of the gas. Even though, the reported dimming range is 100:1, its control scheme used is complicated [B41].

2.5 Motivations and Objective

The existing single-stage ballast still uses two different switches, and two different drives for the low side switch and the high side switch. The loss is also high due to two-time possessing of energy and the switching losses. Finally, due to the fact that the only reduction from the two-stage scheme is in one switch, the component count is still high which decreases the reliability and increases the cost. In this research we will propose a circuit that alleviates these issues. The goal is to achieve soft switching, using one switch while meeting the entire ballast design requirement:

1) High power factor.

2) Low total harmonic distortion.

3) Low electromagnetic interference (EMI).

4) Low lamp current crest factor.

5) Low flickering.

6) Dimming capability.

7) High efficiency.

8) Low components count.

CHAPTER 3

SINGLE SWITCH ZERO VOLTAGE BALLAST

3.1 Introduction

In this Chapter, the proposed new circuit will be synthesized from the typical class D inverter discussed in Chapter 2. It will be shown that the new inverter topology has both the benefit of class D's stable output current, and class E's single-switch zero voltage switching. The new circuit will be analyzed and conditions for zero-voltage switching will be given. Component stress analysis will be carried out. Different dimming methods using the new circuit will be explored. Simulation and experimental verification of the proposed topology will be given and compared. Benefit and draw back observed in the new topology will be highlighted.

3.2 Circuit Synthesis

The series parallel inverter (SPRI) shown in Fig. 3-1(a) has been extensively studied in the literature [C1-C6]. The inverter is composed of two bi-directional switches and a resonant tank circuit L-C1-C2-RL, where RL is the equivalent AC load resistance of the Lamp. If capacitor C1 is very large (DC blocking capacitor) the inverter becomes a Parallel Resonant Inverter (PRI).

Fig. 3-1 (b) shows transformation of the parallel combination of the load RL and the C2 to a series combination R_s, C_s. The two switches are turned on and off alternatively, at the

switching frequency $f_s = \frac{\omega_s}{2\pi}$ with a variable duty cycle. The tank voltage sees a pulse that switches from V_{dcin} to 0 as shown in Fig. 3-1(c). By transforming the pulse V_{dcin} voltage source and capacitor C1 from a series combination to a parallel combination, we obtain Fig. 3-2 (a). Rearranging the component and adding a circuit to create a current source, we obtain the initial proposed circuit Fig. 3-2 (b). The circuit obtained has the main benefit of a class-E inverter [C8-C18]. The class-E amplifier, first proposed by Sokal and Sokal [C8], [C9], is a resonant switch-mode circuit where switching losses are eliminated in the optimum operating conditions of zero-voltage switching (ZVS) and zero-current switching (ZCS) at turn on. The class-E amplifier is therefore a prime candidate for efficient operation at high switching frequencies. The circuit is simple, typically using one switch coupled to a resonant network as shown in Fig. 3.2 (b). On the other hand, it has two major differences in the mode of operation. First, the input inductor L is finite, so no constant DC current source can be assumed in the input. Second, capacitor C_s is large enough to assume a constant DC source. Using the above assumption, the circuit can be shown to have four modes of operation.

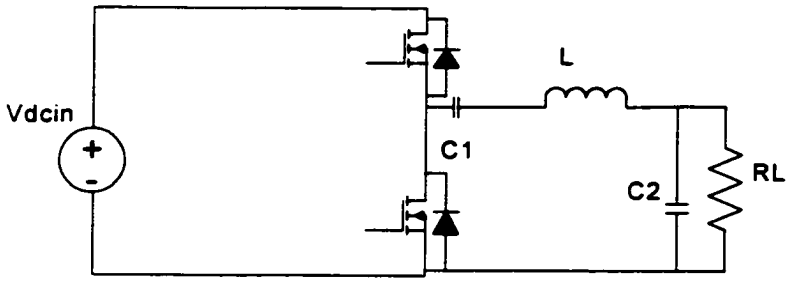

(a)

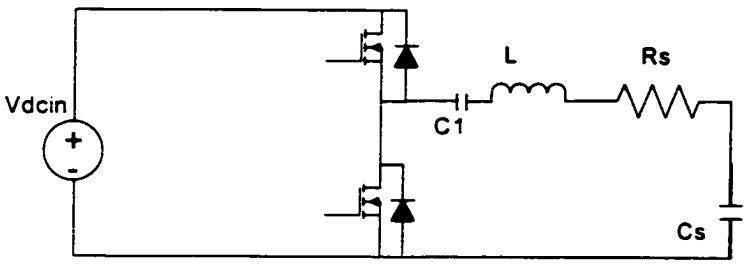

(b)

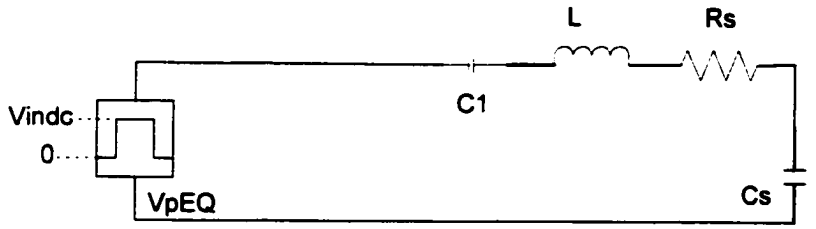

(c)

Figure 3-1 Equivalent Circuit of the Series Parallel Resonant Inverter

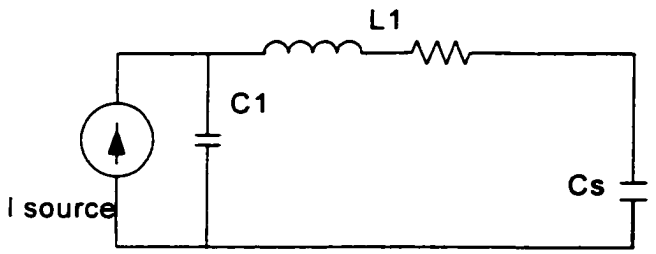

(a)

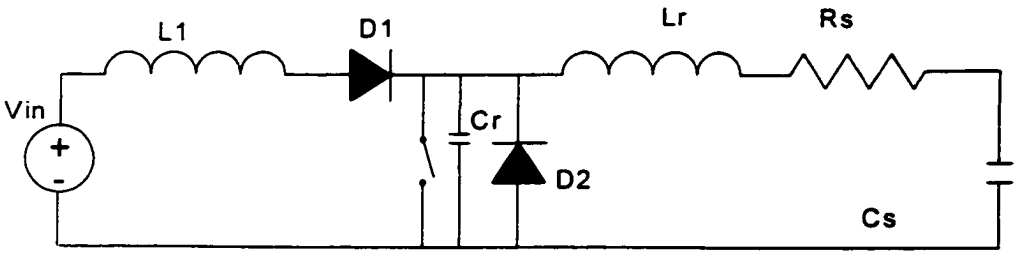

(b)

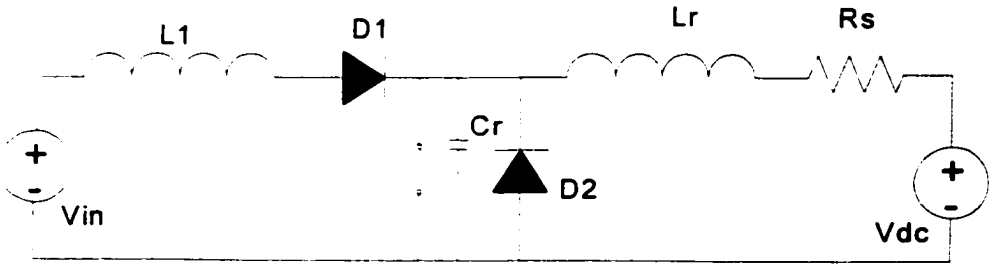

(c)

Figure 3-2 Proposed Circuit Synthesis

3.3 Circuit Analysis

It can be shown that the circuit has a total of four modes of operation.

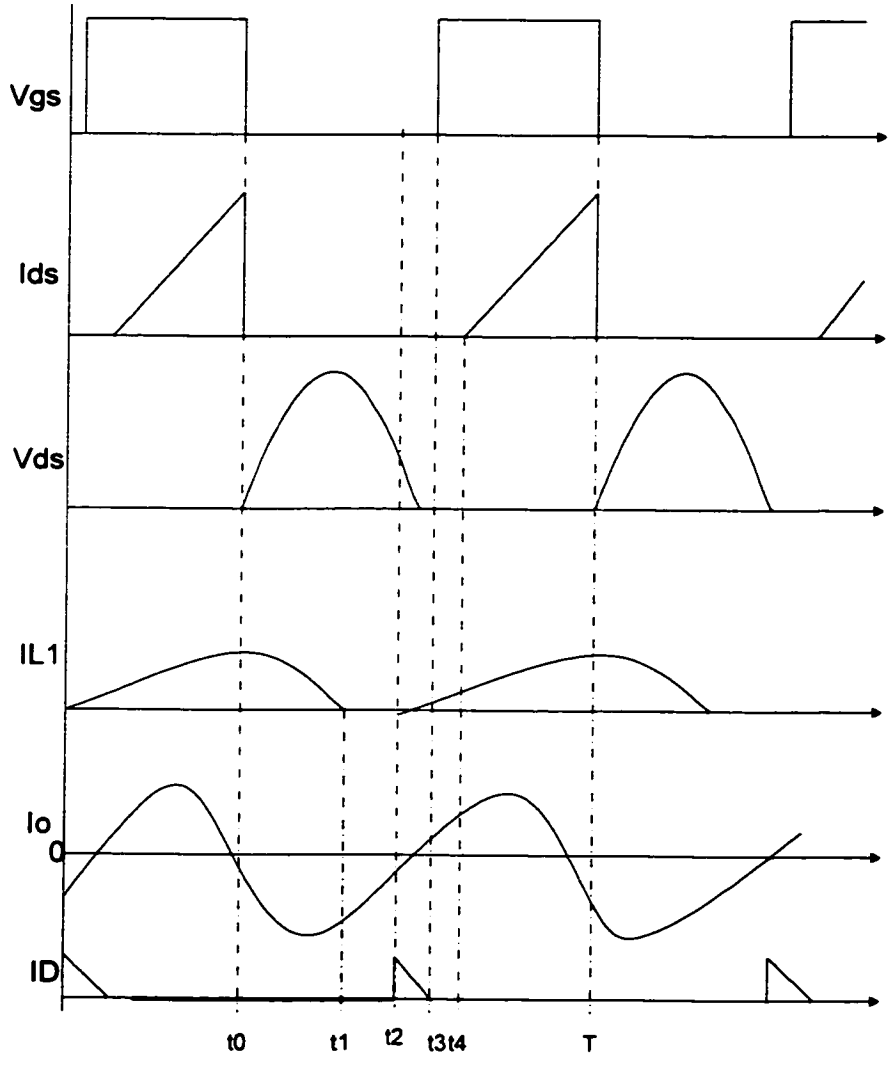

Figure 3-3 Different Operation Waveforms

We will start the mode of operations assuming the switch was on, and then at $t = t_0$ it was turned off.

Mode 1 $t_0 \le t \le t_1$

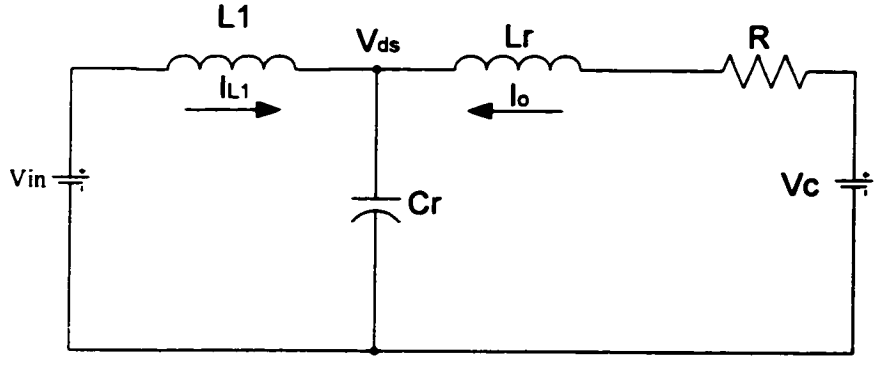

Figure 3-4 Equivalent Circuits in Mode 1

Let us assume that the main switch turns off at t_0. Because of the parallel resonant capacitor, C_r, the voltage across the main switch will not change rapidly, so it turns off under the zero-voltage condition. The current in the boost choke L_1 and load inductor L_r act as current sources. Both sources will charge the capacitor C_r and cause the V_{ds} to increase resonantly. As was mentioned before, the goal is to have the boost inductor operating in discontinuous mode in order to achieve high power-factor correction. So, all the power will be transferred to the load before the next cycle. The power stored in the choke inductor L_1 is transferred to C_r. At t_1, i_{L1} decreases to zero. All energy stored in L1 during the switch-on period is transferred to C_r. Because of blocking diode D1, i_{L1} will be zero until the next cycle. Therefore, we obtain:

$$C_r \frac{dv_{ds}(t)}{dt} = i_{L1}(t) + i_0(t) \tag{3-1}$$

$$L_r \frac{di_0(t)}{dt} + v_{ds}(t) + Ri_0(t) = V_{in} \tag{3-2}$$

$$L_1 \frac{di_{L1}(t)}{dt} = V_{in} - V_{ds}(t) \tag{3-3}$$

With the following initial conditions:

$v_{ds}(0) = 0. i_0(0) = I_o$. and $i_{L1}(0) = I_1$

This mode will end when the input inductor current reaches zero.

Mode 2 $t_1 \le t \le t_2$

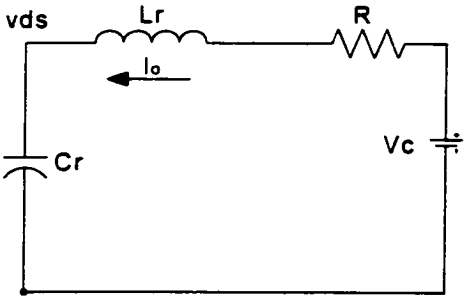

Figure 3-5 Mode 2 of Operation

In this mode, the output inductor L_r and resonant capacitor C_r forms a series resonant circuit. Because the voltage across C_r is now higher than the voltage across the storage capacitor, the load current increases in the reverse direction, which transfers the power from C_r to load and storage capacitor C_s. At t_2, V_{ds} becomes less than the input

voltage V_{in} so diode D_1 can conduct, and the boost inductor starts charging up again. The governing equations in this mode are given by,

$$C_r \frac{dv_{ds}(t)}{dt} = i_o(t) \tag{3-4}$$

$$L_r \frac{di_0(t)}{dt} + v_{ds}(t) + Ri_o(t) = V_{dc} \tag{3-5}$$

This mode will end when the voltage $v_{ds} = V_{in}$ at $t = t_2$

Mode 3 $t_2 \le t \le t_3$

This mode starts when the drain-to-source voltage becomes lower than the input voltage so diode D_1 starts conducting. The equivalent circuit in

Mode 1 is as shown in Fig 3-4. The mode will be governed by the same equation as mode 1; the only difference is the initial condition.

$$C \frac{dV_{ds}(t)}{dt} = i_{L1}(t) + i_o(t) \tag{3-6a}$$

$$L_r \frac{di_o(t)}{dt} + v_{ds}(t) + Ri_o(t) = V_{dc} \tag{3-7a}$$

$$L_1 \frac{di_{L1}(t)}{dt} = V_{in} - v_{ds}(t) \tag{3-8a}$$

The following initial condition will apply:

$i_{L1}(t_2) = 0$

Mode 4 $t_3 \le t \le T$

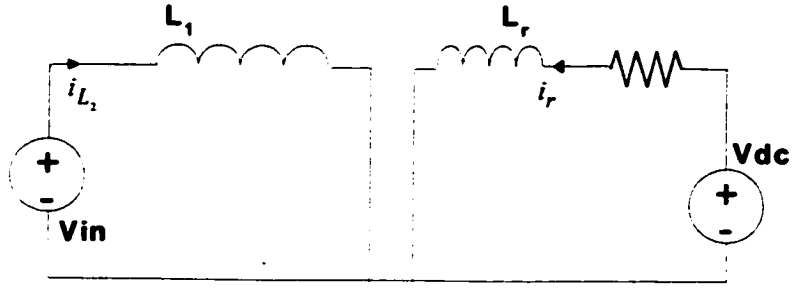

Figure 3-6 Mode 4 of Operation

In this mode the switch will be turned on and both inductors will charge up linearly. The action of the input inductor L_1 is similar to the typical boost inductor that will be charged up to feed the load when the switch is off; on the other hand the resonant inductor will continue to charge.

$$L_1 \frac{di_{L1}(t)}{dt} = V_{in} \qquad (3\text{-}9a)$$

$$L_r \frac{di_o(t)}{dt} + i_o(t) = V_{dc} \qquad (3\text{-}10a)$$

3.4 Analytical Solutions

In order to gain more insight into the circuit, the analytical solution will be carried out with the some assumption. Since the resonant cap across the switch is in the order of nanofarads, it will charge rapidly when the switch is open. Second, Mode 3 is very short compared to the rest of the period, so we will assume that the input inductor stays at zero

until the next switching cycle. Using these assumptions, the circuit could be studied as a two-mode circuit.

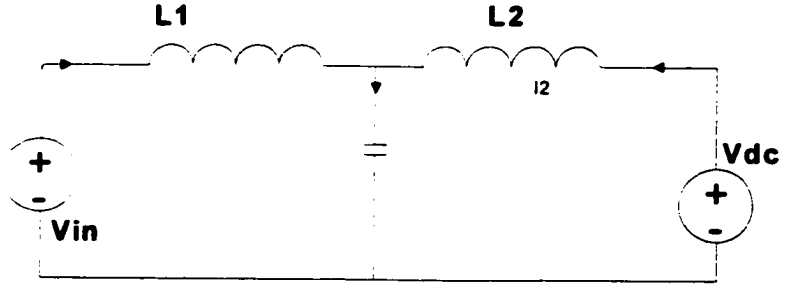

Figure 3-7 Equivalent Circuit in Mode 1

This is the mode where the switch is turned off:

We will also assume a high output quality factor high enough so that the output load current is sinusoidal.

$$i_o(t) = I_o \operatorname{Sin}(\omega t + \phi) \tag{3-1}$$

$$0 \le t \le \frac{\pi}{\omega}$$

$$V_{dc} - Ri_o(t) - L_r \frac{di_o}{dt} = v_c(t) \tag{3-2}$$

$$V_{in} = L_1 \frac{di_1}{dt}(t) + v_c(t) \tag{3-3}$$

$$C \frac{d}{dt} V_c(t) = i_0(t) + i_1(t) \tag{3-4}$$

Where $i_o(t)$ is the output current, $v_{c(t)}$ is the voltage across C_r

and $i_o(t)$ is the current through the boost inductor L_1, when the switch is off.

Using Eq. (3-3), (3-4) we get the second order equation:

$$L_1 C \frac{di_1^2}{dt^2}(t) + \frac{di_1}{dt}(t) + I_o \operatorname{Sin}(\omega t + \phi) = o \tag{3-5}$$

The solution can be shown in the form:

$$i_1(t) = \left(A\cos(\omega_o t) + B\sin(\omega_o t)\right) - \frac{I_o \sin(\omega t + \phi)}{1 - \beta^2} \tag{3-6}$$

And from Eq. (3-3) we have:

$$v_c(t) = -L_1\left[- A\sin(\omega_o t)\omega_o + B\cos(\omega_o t)\omega_o - I_o \cos(\omega t + \phi)\frac{\omega}{(1 - \beta^2)}\right] + V_{in} \tag{3-7}$$

where,

$$\omega_o = \frac{1}{\sqrt{L_1 C}} \qquad \beta = \frac{\omega}{\omega_o}$$

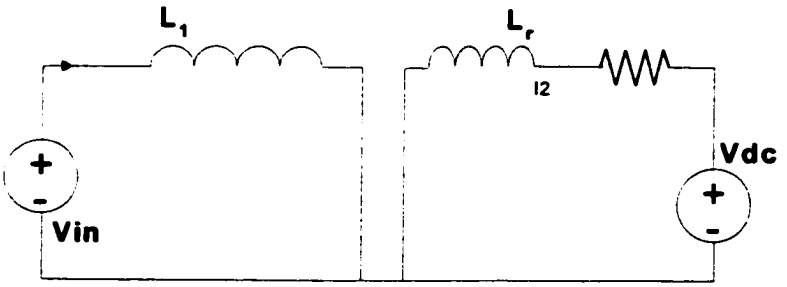

Fig. 3-8 Equivalent Circuit in Mode 2

Mode 2 is when the voltage across the cap goes to zero and the anti-parallel diodes start conducting.

Mode 2:

$$\frac{\pi}{\omega} \leq t \leq \frac{2\pi}{\omega}$$

$$V_{in} = L_1 \frac{di_1}{dt}(t) \tag{3-8}$$

$$V_{dc} - Ri_o(t) - L_r \frac{di_o}{dt}(t) = c \tag{3-9}$$

The solution for Eqs. (3-8) and (3-9) are:

$$i_1(t) = \frac{V_{in}}{L_1}(t - \tfrac{\pi}{\omega}) + \gamma \tag{3-10}$$

$$i_o(t) = \frac{v_{dc}}{R} + \lambda e - R\frac{t}{L_2} \tag{3-11}$$

From the above equations and the boundary condition we can solve for A, B, γ, λ, I_o, and Φ .

The boundary conditions will be stated as:

$$i_1\left(2\frac{\pi}{\omega}\right) = i_1(o) \tag{3-12}$$

$$i_1\left(\frac{\pi}{\omega}\right) = i_1\left(\frac{\pi}{\omega}\right) \tag{3-13}$$

$$V_c(0) = 0 \tag{3-14}$$

From Eq. (3-6) and (3-10)

we obtain:

$$i_1(0) = A - I_0 \frac{\sin(\phi)}{1-\beta^2} \tag{3-15}$$

$$i_1\left(2\frac{\pi}{\omega}\right) = \frac{V_{in}}{L_1}\frac{\pi}{\omega} + \gamma \tag{3-16}$$

$$i_1\left(\frac{\pi}{\omega}\right) = A\cos\left(\omega_o \frac{\pi}{\omega}\right) + B\sin\left(\omega_o \frac{\pi}{\omega}\right) + I_0 \frac{\sin(\phi)}{\left(1-\beta^2\right)} \tag{3-17}$$

$$i_1\left(\frac{\pi}{\omega}\right) = \gamma \tag{3-18}$$

From Eq. (3-7) and (3-14) we obtain:

$$V_{in} = L_1\left[B\frac{\omega}{\beta} - I_0\cos(\phi)\frac{\omega}{1-\beta^2}\right] \tag{3-19}$$

From Eq. (3-15) and (3-16) and condition (3-12)

we obtain:

$$\frac{V_{in}}{L_1}\frac{\pi}{\omega} + \gamma = A - I_0\frac{\sin(\phi)}{1-\beta^2} \tag{3-20}$$

From Eq. (3-17) and (3-18) and condition (3-13) we obtain

$$\gamma = \left(A\cos\left(\frac{1}{\beta}\pi\right) + B\sin\left(\frac{1}{\beta}\pi\right)\right) + I_0\frac{\sin(\phi)}{\left(1-\beta^2\right)} \tag{3-21}$$

Solving Eq. (3-19) to (3-20) for γ, A, and B as function of β, Φ and I0 we have:

$$B = \beta \frac{\left(-V_{in} + V_{in}\beta^2 - L_1\omega I_0 \cos(\phi)\right)}{\left[L_1\omega\left(-1+\beta^2\right)\right]} \tag{3-22}$$

$$A = \frac{\left(-\beta^3 \sin\left(\frac{1}{\beta}\pi\right)V_{in} - V_{in}\pi\beta^2 + \beta\sin\left(\frac{1}{\beta}\pi\right)V_{in} + \beta\sin\left(\frac{1}{\beta}\pi\right)L_1\omega I_0\cos(\phi) + 2I_0\sin(\phi)L_1\omega + V_{in}\pi\right)}{\left[\left(1-\beta^2-\cos\left(\frac{1}{\beta}\pi\right)+\cos\left(\frac{1}{\beta}\pi\right)\beta^2\right)L_1\omega\right]} \tag{3-23}$$

$$\gamma := \frac{\left(-\beta^3\cdot\sin\left(\frac{1}{\beta}\cdot\pi\right)\cdot Vin - Vin\pi\cdot\beta^2 + \beta\cdot\sin\left(\frac{1}{\beta}\cdot\pi\right)\cdot Vin + \beta\cdot\sin\left(\frac{1}{\beta}\cdot\pi\right)\cdot L1\cdot\omega\cdot I0\cdot\cos(\phi) + 2\cdot I0\cdot\sin(\phi)\cdot L1\cdot\omega + Vin\pi\right)}{\left[\left(1-\beta^2-\cos\left(\frac{1}{\beta}\cdot\pi\right)-\cos\left(\frac{1}{\beta}\cdot\pi\right)\cdot\beta^2\right)\cdot L1\cdot\omega\right]} - \left[I0\frac{\sin(\phi)}{\left(1-\beta^2\right)} + \frac{Vin\pi}{L1\ \omega}\right] \tag{3-24}$$

Using the condition stated for zero-voltage switching and zero current in the input inductor at switching, we obtain:

$$V_c\left(\frac{\pi}{\omega}\right) = 0 \tag{3-25a}$$

$$i_1\left(\frac{\pi}{\omega}\right) = 0 \tag{3-25b}$$

Using (3-7) and condition (3-25) we can solve for I0 as a function of ϕ and β

$$V_c\left(\frac{\pi}{\omega}\right) = -L_1\left[-A\sin\left(\frac{\pi}{\beta}\right)\omega_o + B\cos\left(\frac{\pi}{\beta}\right)\frac{\omega}{\beta} + I_0\cos(\phi)\frac{\omega}{\left(1-\beta^2\right)}\right] + V_{in} \tag{3-26}$$

Then, using condition (3-25) and Eq. (3-24) one can solve for ϕ as function of β

$$I_0 = V_{in} \frac{\left(\beta^3 \sin\left(\frac{1}{\beta}\pi\right) + \pi\cos\left(\frac{1}{\beta}\pi\right)\beta^2 - \beta\sin\left(\frac{1}{\beta}\pi\right) - \pi\cos\left(\frac{1}{\beta}\pi\right)\right)}{\left[L_1\omega\left(\beta\sin\left(\frac{1}{\beta}\pi\right)\cos(\phi) + \sin(\phi)\cos\left(\frac{1}{\beta}\pi\right) + \sin(\phi)\right)\right]}$$

(3-27)

$$\phi = a\tan\left[\frac{\left(\sin\left(\frac{1}{\beta}\pi\right)^2 \omega_o\pi\beta + 2\omega\beta\sin\left(\frac{1}{\beta}\pi\right) + \omega\pi - \omega\pi\sin\left(\frac{1}{\beta}\pi\right)^2 + \omega\pi\cos\left(\frac{1}{\beta}\pi\right)\right)}{\left[\sin\left(\frac{1}{\beta}\pi\right)\left(\sin\left(\frac{1}{\beta}\pi\right)\omega - \omega\sin\left(\frac{1}{\beta}\pi\right) - \frac{\omega\pi}{\beta}\right)\right]}\right]$$

(3-28)

In order to analyze the stress on the component, we will normalize the above relation as follows. The current will be normalized by $\frac{V_{in}}{L_1\omega}$, the voltages will be normalized by V_{in} , and all the impedance by $L_1\omega$. Using this procedure the above equations became:

$$B_{n(\beta)} = -\beta\frac{\left(1 - \beta^2 + I_0 n(\beta)\cos(\phi(\beta))\right)}{\left(-1 + \beta^2\right)}$$

(3-29)

$$A_n(\beta) = \frac{-\beta^3 \sin(\frac{1}{\beta}\pi) + \pi\beta^2 - \beta\sin(\frac{\pi}{\beta}) - \beta\sin(\frac{\pi}{\beta})I_{on}(\beta)}{1 - \beta^2 - \cos(\frac{\pi}{\beta}) + \cos(\frac{\pi}{\beta})\beta^2}$$
$$\frac{-2I_{on}(\beta)\sin(\phi(\beta)) - \pi}{1 - \beta^2 - \cos(\frac{\pi}{\beta}) + \cos(\frac{\pi}{\beta})\beta^2}$$

(3-30)

$$\phi(\beta) = -a\tan\left[\left(2\beta\sin\left(\frac{1}{\beta}\pi\right)+\pi+\pi\cos\left(\frac{1}{\beta}\pi\right)\right)\frac{\beta}{\left(\sin\left(\frac{1}{\beta}\pi\right)\pi\right)}\right]$$

(3-31)

$$i_{1n}(\beta,\omega,t) = \left(A_n(\beta)\cos\left(\frac{\omega}{\beta}t\right)+B_n(\beta)\sin\left(\frac{\omega}{\beta}t\right)\right)-\frac{I_{0n}(\beta)\sin(\omega t+\phi(\beta))}{\left(1-\beta^2\right)}$$

(3-32)

Substituting the above equations into Eqs. (3-6) and (3-7) one can get the normalized switch voltage as a function of β and γ.

$$V_{cn}(\beta\omega) = 1-\left[\left(-A_n(\beta)\right)\sin\left(\frac{\omega}{\beta}t\right)\frac{1}{\beta}+B_n(\beta)\cos\left(\frac{\omega}{\beta}t\right)\frac{1}{\beta}-I_{0n}\cos(\omega t+\phi(\beta))\frac{1}{1-\beta^2}\right]$$

(3-33)

And the normalized output current peak is:

$$i_{0n}(\beta) = \frac{\left(\beta^3\sin\left(\frac{1}{\beta}\pi\right)+\pi\cos\left(\frac{1}{\beta}\pi\right)\beta^2-\beta\sin\left(\frac{1}{\beta}\pi\right)-\pi\cos\left(\frac{1}{\beta}\pi\right)\right)}{\left(\left(\beta\sin\left(\frac{1}{\beta}\pi\right)\cos(\phi(\beta))+\sin(\phi(\beta))\cos\left(\frac{1}{\beta}\pi\right)+\sin(\phi(\beta))\right)\right)}$$

(3-34)

Evaluating the Eq. (3-33) at a quarter of the switching frequency $\frac{\pi}{2\omega}$, we get an equation that depends only on the rapport of the switching frequency to the resonant frequency. Plotting the equation as a function of β and ω.

$$V_{cn}(\beta) = 1 + A_n(\beta)\frac{\sin\left[\frac{1}{(2\beta)}\pi\right]}{\beta} - B_n(\beta)\frac{\cos\left[\frac{1}{(2\beta)}\pi\right]}{\beta} - I_{0n}(\beta)\frac{\sin(\phi(\beta))}{1-\beta^2}$$

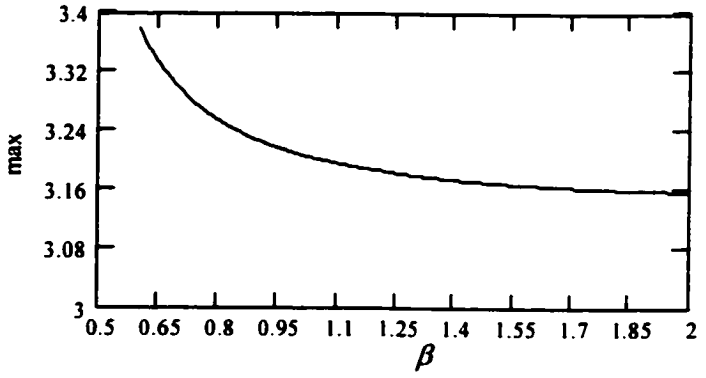

Figure 3-9 (a) Maximum v_{ds} (t) as Function of β

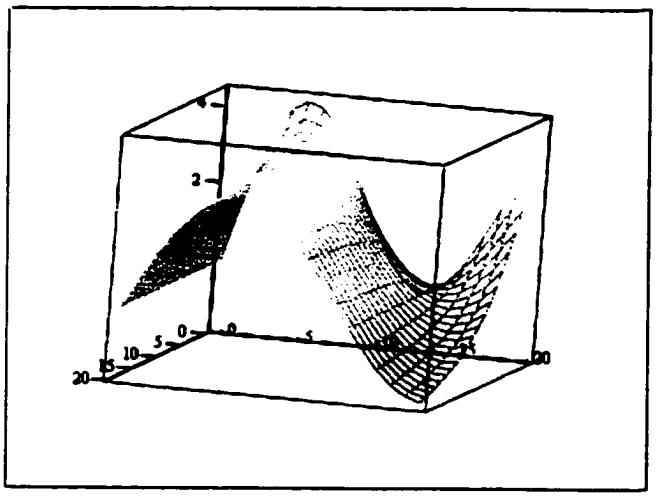

Figure 3-9 (b) v_{ds} (t) as Function of β and ω

3.5 Design Example and Experimental Verification:

The design can be carried out as follows. First, a $\beta = 0.9$ was chosen to achieve low drain-to-source voltage. Then, a switching frequency of 30kHz and peak input current of 1A were also chosen. Using Eq. (3-32) at t=0 and $\beta = 0.9$

We obtain the normalized input current equal to 3.2. The component using V_{in}= 160, and L_2=1.4mH are then obtained.

$$L_1 = \frac{32V_{in}}{\omega}$$

L_1= 2.7mH, and using $\omega_o = \frac{\omega}{\beta}$ we have $\omega_o = 9.4 \times 10^4$.

Then we used $\omega_o = \frac{1}{\sqrt{L_r C_r}}$ to get the value of C= 15nF

A Pspice simulation circuit using the above values was setup. In the simulation a resistor was used as the lamp model.

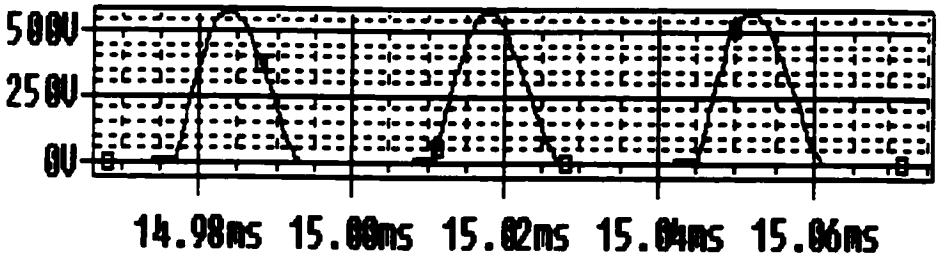

(a)

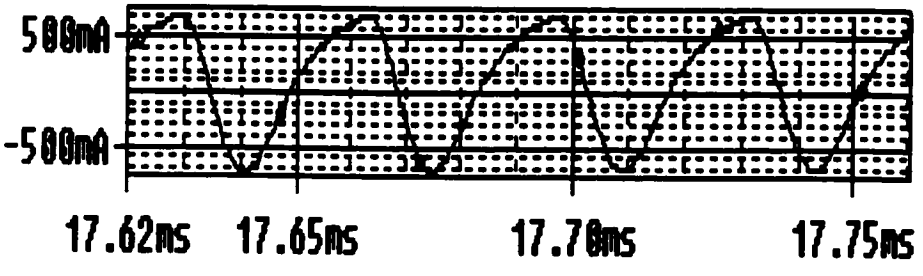

(b)

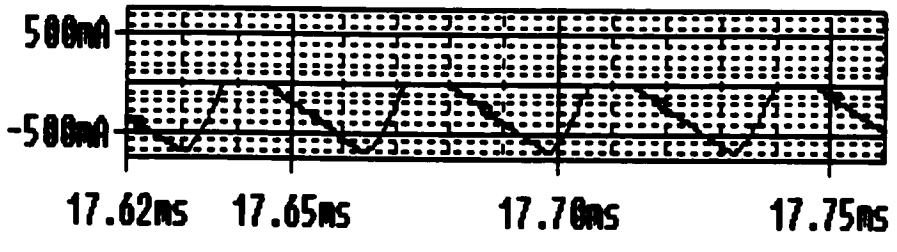

(c)

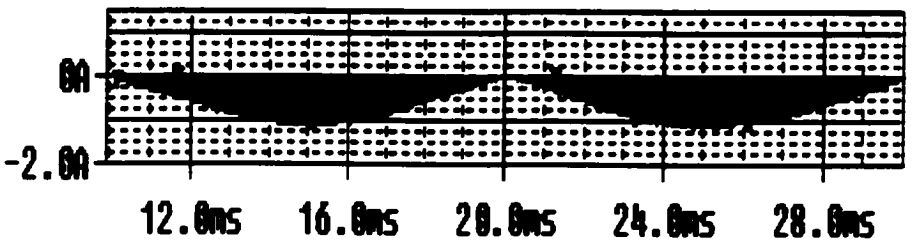

(d)

Fig 3-10 (a) The Drain to Source Voltage (b) The Output Current (c) Input Inductor Current and (d) Input Current During the Full Cycle.

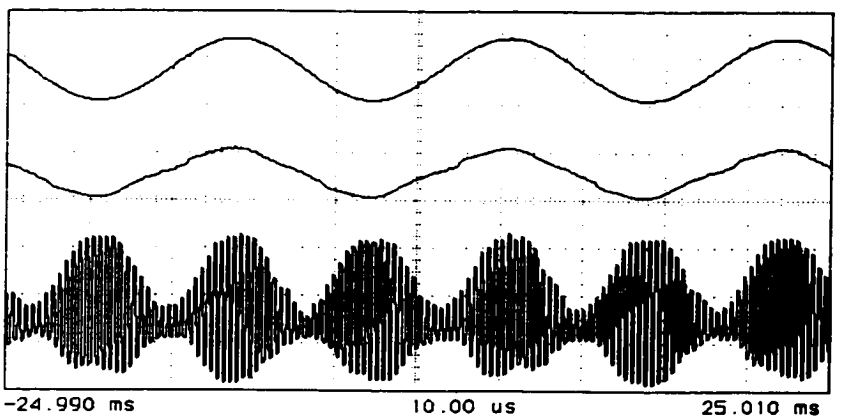

Figure 3-11 Experimental Lamp Current Waveform.

As can be observe from the simulation results, we were able to achieve high power factor and zero voltage switching. Using the same values, the experimental result was carried out and all the expected results were achieved. Other than the lamp current as shown in Fig. 3-11, we noticed discontinuity in the current and a 50 Hz cycle envelope.

Using the following worst-case-scenario waveform from the output current, we obtain:

Fig- 3-12 Lamp Current Waveform for Crest Factor Approximation.

$$i_o(\theta,\rho) = I_o \sin(\theta)\sin(\rho) \tag{3.35}$$

where,

θ is the angular line frequency and ρ is the angular switching frequency.

Knowing that switching frequency is a lot higher that the line frequency, the RMS current could be calculated as follows:

$$I_{rms} = \sqrt{\frac{1}{2\pi}\int_0^{2\pi}\left[\sqrt{\frac{1}{2\pi}\int_0^{2\pi}\left(I_o \sin(\theta)\sin(\rho)\right)^2 d\rho}\right]d\theta} \tag{3.36}$$

so, $= \frac{I_o}{2}$

so the CF is 2.

This discrepancy resulted from our use of a simple resistor as a model for the lamp. Two major efforts must be carried out in order for us to meet the requirement. First, we need to achieve a better crest factor and also develop a more accurate lamp model.

CHAPTER 4

IMPROVED CIRCUIT AND MODEL

4.1 Crest Factor Improvement

The lamp manufacturer normally suggests that the crest factor of the filament does not exceed 1.7. The crest factor is defined as:

$$CF = \frac{\text{Peak Lamp Current}}{\text{RMS Lamp Current}}$$

This is an important parameter in the lamp operating life. To achieve the desired crest factor, two methods will be discussed and analyzed. The first consists of a valley fill as shown in Fig. 4-1(a), and the second is the combination of the valley fill and frequency modulation as shown in Fig. 4-1(b), when $V_{in}(t)$is the input voltage.

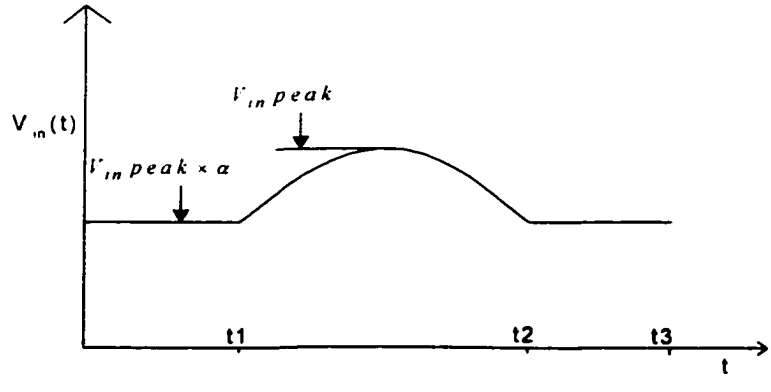

(a)

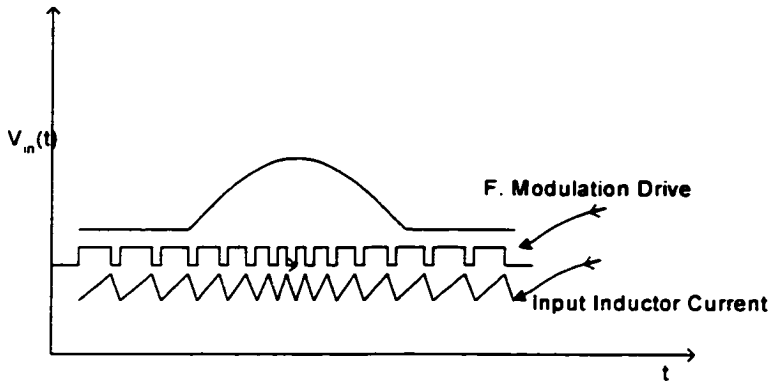

(b)

Figure 4-1(a) Valley Fill (b) Valley Fill with Frequency Modulation.

4.1.1 Valley Fill Methods

From Fig. 3-6 we can see that the output current shows a waveform envelope reflecting the input rectified voltage. From that observation, the crest factor can be reduced if the contour of the lamp current becomes flat.

The first proposed method is to reduce the difference between the RMS and the peak current of the lamp by super imposing a DC voltage at the input side of the inverter, which will decrease the difference between the input voltage RMS and peak. In this method, an extract winding will be added to the input inductor as shown in Fig. 4-2 (a).

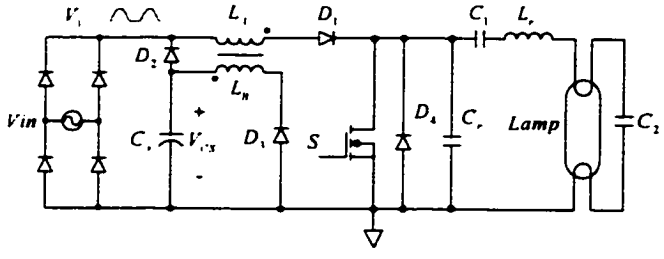

(a)

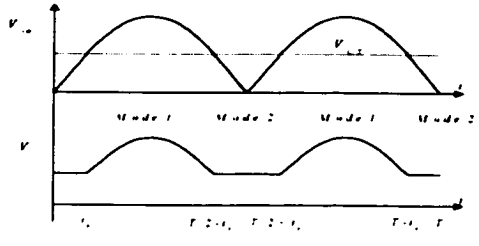

(b)

Figure 4-2 Valley Simplified Circuit and Input Waveforms.

This winding will supply the input voltage when the input AC voltage falls below a predesigned value. Using Fig. 4-1(a).

$$I_{Peak} = \frac{V_{indc} T_{on}}{L} = \frac{V_{indc} DT}{L} \qquad (4\text{-}1)$$

Where,

V_{indc} is the input voltage seen by the inductor, D is the duty cycle, and T is the switching period.

When the switch is turned off, the inductor will discharge to zero:

$$T_{off} = \frac{I_{pk} L}{(V_{out} - V_{in} dc)} \tag{4-2}$$

The average

$$I_{on(ave)} = \frac{V_{in} dc D^2 T}{2L} \tag{4-3}$$

$$I_{off(ave)} = \frac{V_{in} dc^2 D^2 T}{2L(V_{out} - V_{in} dc)} \tag{4-4}$$

Using (4-3) and (4-4) we obtain:

$$I_{in(ave)} = \frac{V_{in} dc V_{out} D^2 T}{2L(V_{out} - V_{in} dc)} \tag{4-5}$$

$$\zeta \equiv \frac{D^2 T V_{out}}{2L} \text{ And } \alpha = \frac{Vm}{V_{out}} \tag{4-6}$$

$$P_{in} = \frac{1}{\pi} \int_0^{\pi} V_{in} I_{in} d\theta \tag{4-7}$$

Knowing that,

For $t_1 < t < t_2$

$I_{in}(\theta) = I_{inavr}$

$$t_0 < t < t_1 \text{ and } t_2 < t < \frac{\pi}{\omega}$$

$$I_{in}(\theta) = 0$$

$$t_1 < t < t_2 \qquad (4\text{-}9)$$

So (4-7) became:

$$P_{in} = \frac{1}{\pi} \times \int_{\theta 1}^{\pi - \theta 1} Vm \times \sin(\theta) \times \zeta \times \left(\frac{\alpha \times \sin(\theta)}{1 - \alpha \times \sin(\theta)}\right) \times d\theta \qquad (4\text{-}10)$$

where,

$$\theta_1 = \omega t_1 \text{ and } \theta = \omega t$$

In order to get the power factor correction as a function of $\theta_1 = \omega t_1$, we need the RMS value of the current.

$$i_{rms} = \sqrt{\frac{1}{\pi} \int_0^{\pi} I_{in}^2 d\theta}$$

$$PF = \frac{P_{in}}{V_{rms} I_{rms}} = \frac{\sqrt{2P_{in}}}{V_m i_{rms}} \qquad (4\text{-}11)$$

An Analytical equation is too complicated and does not give any insight into the circuit optimization, so the above equations were simplified and numerically solved in Fig 4-3.

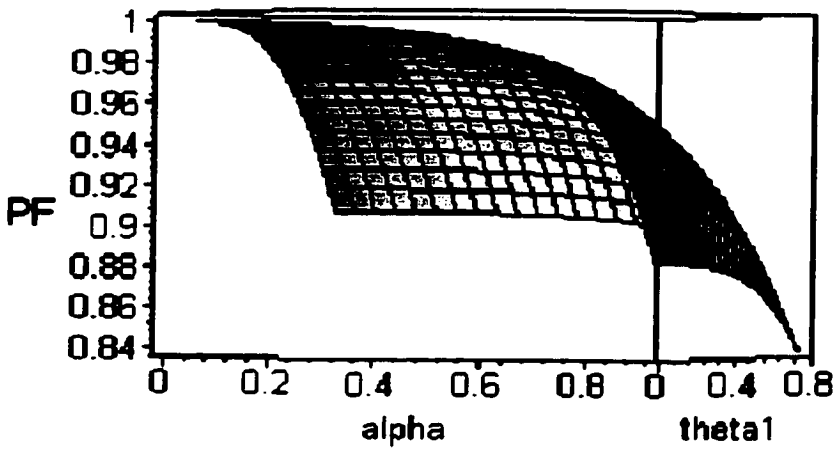

Figure 4-3 Power Factor Correction as a Function of the Ratio of α *and* θ1

From Fig. 4-3 we can see that even as θ_1 moves close to $\frac{\pi}{4}$, we can still achieve a high PF. The PF requirement for ballast application is more that 94 percent. So, we can choose $\theta_1 = \frac{\pi}{8}$ and α can still be chosen more that 0.8 to achieve low voltage stress on the switch. Using the circuit proposed in Fig. 4-2 (a) without the valley fill circuit, the result is shown in Fig. 4-4 (a). It has Power factor 0.992 (THD = 9%), Lamp current Crest factor ≈2 after adding the valley fill circuit, and we can see clearly that the Power factor is 0.972 (THD = 20.5%). We see from the above result that we still need to improve the crest factor. The proposed method is to reduce the difference between the peak and RMS

values of lamp current by decreasing the fluctuation of the contour of the lamp current. In this scheme, an FM switching technique based on the DC-link voltage waveform is used to reduce the fluctuation difference. When the valley part of the DC-link voltage is applied to the lamp, the switching frequency of the inverter decreases to a preset value to increase the magnitude of the lamp current. Note that such an increase of the supplied lamp current is accomplished by increase of the voltage-boost-gain resonant-inverter circuit. When the hill part in the DC-link voltage is applied to the lamp, the switching frequency increases with the shape of the voltage up to a preset value, and consequently makes the lamp current decrease. The idealized waveform of the lamp current can be changed from the concave contour of Fig. 4-4 (a), to a more uniform current waveform. Therefore, the crest factor of the lamp current becomes smaller. The DC-link voltage waveform can be used as the basic reference waveform for the control input signal of the proposed method. The experimental result carried out using this method showed a major improvement of the crest factor in Fig. 4-4 (c).

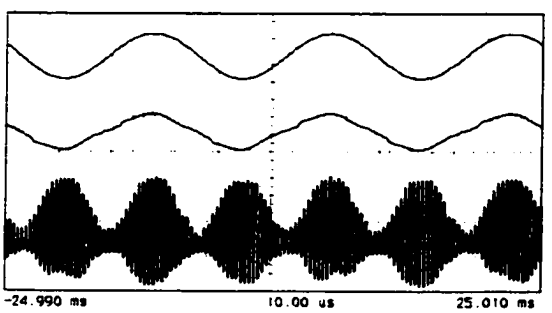

(a) Line and Lamp Current Waveforms of Basic Class E Ballast

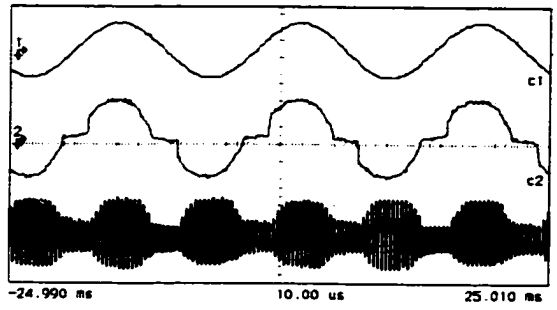

(b) Without Duty Cycle Modulation Control Method

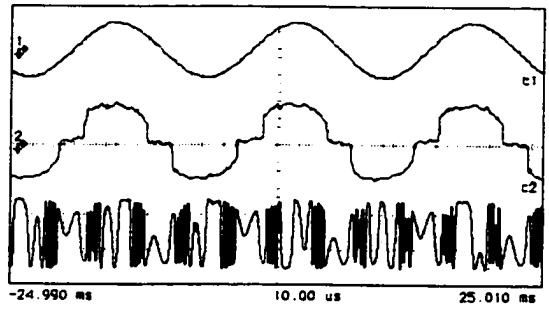

(c) With Duty Cycle Modulation Control Method

Figure 4-4 Line and Lamp Current Waveforms of Valley Fill and Frequency Modulation

4.2 Modeling of Fluorescent Lamps for Dimming Operation

Lamp behavior must be well studied in order to properly design and control the electronic ballasts. The first approach used was to model the lamp as resistance [D1-D2]. A major discrepancy between the experimental and the simulation results was observed. This approach is valid for only one operating point since, in the normal operating range, the lamp's effective resistance decreases at higher lamp current and increases at lower lamp current as shown in Fig 4-5.

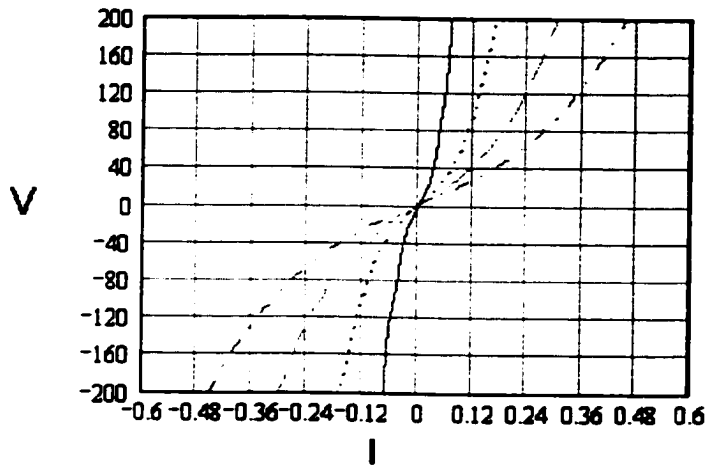

Figure 4-5 I/V Characteristic of the Lamp.

An improvement over a fixed-resistance model is to make the lamp resistance a function of the average lamp power. Many models were presented in the literature [D3-D9]. A simple model is one that varies lamp resistance [D3] in a way that produces a lamp voltage that has a constant RMS voltage. A more elaborate variable-resistance model, based on physical lamp properties, is described in [D4]. The model proposed here uses a cubic function of the lamp voltage and the lamp current.

The equation will be archived as follows:

$$v_L(t) = A(p)i_L(t) + [B(p)i_L(t)]^3 \qquad (4\text{-}12)$$

In order to get the values of A, B we first operated the lamp at different power levels. From these data, we used curve fitting techniques to get the equation representative of A and B as a function of power. The result is as follows:

$$A(p) = \frac{a_1}{p} + a_2 + a_3 \times p + a_4 \times p^2 \tag{4-13}$$

$$B(p) = \frac{b_1}{p} + b_2 + b_3 \times p + b_4 \times p^2 \tag{4-14}$$

The values of a_1 to a_4 and b_1 to b_4 are lamp-type dependent. From these values one can construct a Pspice model for the lamp.

Using the Sylvania lamp T8, the following parameter were obtained (Table 4-1).

Table 4-1 Coefficient Values for T8

a_1	a_2	a_3	a_4	b_1	b_2	b_3	b_4
10468	-431.85	21.641	-.30272	700.7	11.521	-1.1311	.016615

Using the behavioral Pspice model capability, Eqs. (4-12) to (4-13) can be modeled. To verify the proposed model spice, simulation using fixed resistance was carried out in Fig. 4-14 (a,b). This simulation was carried out at full power of the lamp running at frequency of 30kHz.

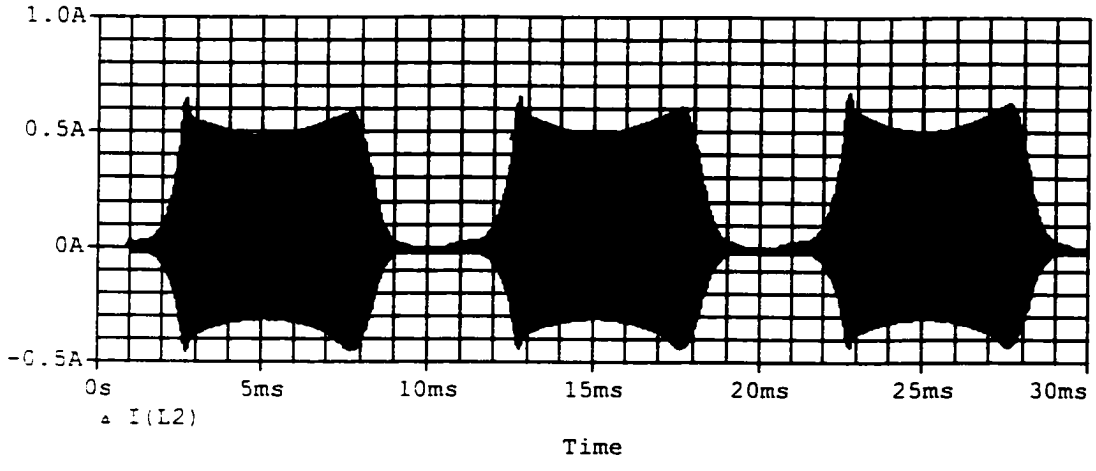

(a) Using the Lamp Model

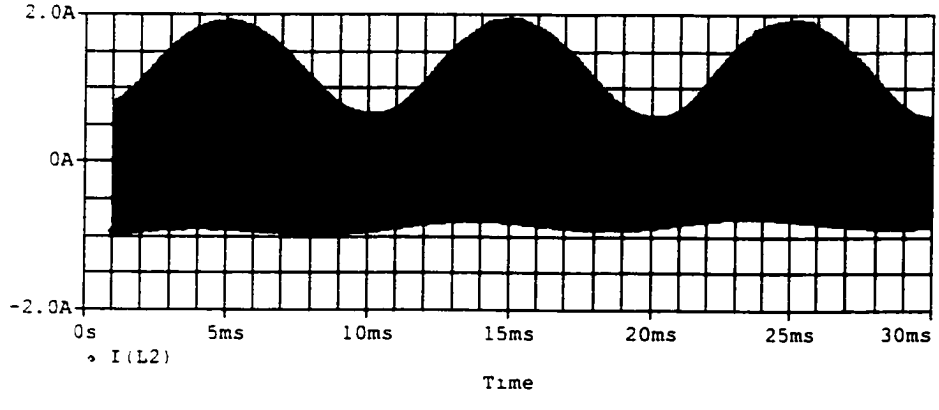

(b) Using a Lamp Resistance of 160Ω

Figure 4-6 Output Lamp Current Simulation

We can see clearly that the use of constant resistance to model the lamp results in wrong lamp-current prediction. The simulation carried out using the proposed lamp model shows the discontinuity that was observed in the experimental result.

CHAPTER 5

ANALYSIS AND COMPARISON OF THE DIFFERENT DIMMING METHODS

As was pointed out in Chapter 2, one of the main advantages of high frequency electronic ballasts is their ability to control the lamp power. Recently, dimming of florescent lamps has become more and more accepted in residential, commercial and industrial lighting applications. The reasons for the popularity of dimming varies from a necessary technology, like in movie theaters and laboratories, to just a method of creating a more comfortable lighting environment, as in residential applications.

5.1 Generalized Method for Dimming

There are two main methods to control the power to the lamp: (a) Constant DC link voltage with variable frequency or (b) variable DC link voltage with constant switching frequency.

5.1.1 Constant DC Link Voltage With Variable Frequency

The constant DC link method is mostly used in the two-stage ballast. The PFC stage provides a regulated DC voltage, for example 400V. The power to the lamp is achieved by varying the inverter frequency, which in turn varies the inverter tank impedance [B40-48]. Although this technique is a sample, it was shown that the sensitivity of the lamp power to the degree of frequency change increased significantly as the power of the lamp fell below 30 percent of its nominal value. Another major drawback of this method is its inability to

control the starting voltage of the lamp. When the lamp is first started, the power factor controller will try to regulate at the predefined voltage. On the other hand, the inverter is running at the starting frequency to get the lamp to arc. The difference between the two frequencies will cause the lamp power to jump.

5.1.2 Variable DC Link Voltage With Constant Frequency

In contrast to the previous method, the variable DC link method has a fixed frequency and uses a variable DC link voltage to achieve lamp power control. This method is comparatively simpler because it only requires that the PFC output voltage stage be controlled to a desired value. This method was shown to have a very limited dimming range if zero voltage or zero current design requirements have to be achieved.

5.2 Dimming Methods for the Proposed Ballast Topology.

In this research, we propose a different method. In order to still have zero voltage switching at all dimming levels, we will fix the off time and vary the on time. To develop a method of dimming the lamp we analyzed the waveforms of Figure 5.1.

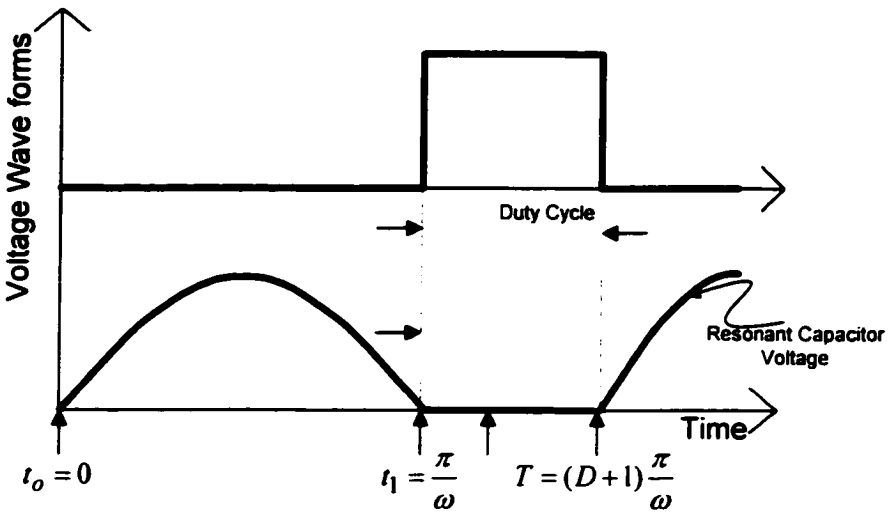

Fig. 5.1 Resonant Capacitor Voltage Through an Entire Cycle

We can see that the mode of operation when the mosfet parallel diode is conducting is similar to the mode of operation when the switch is on. Therefore, the ballast circuit could be analyzed using the previous two modes of operation. We will start the analysis solving Eqs. 3-1 to 3-11 using different boundary conditions. In Chapter 3, the analysis was carried out assuming a worst case situation of 50 percent duty cycle. In the following analysis we will have a variable time on and fixed time off. The following boundary conditions will apply:

$$i_1\left(\frac{\pi}{\omega} + D\frac{\pi}{\omega}\right) = i_1(0) \tag{5-1}$$

$$v_c(0) = 0 \tag{5-2}$$

Where, Vc(t) is the drain to source voltage across the switch, ilon (t) is the input inductor current when the switch in on, and iloff (t) is the input inductor current when the switch is off.

Where:

D is the $\frac{\text{time\_on}}{\text{time\_off}}$

Using Eqs. 5-1 to 5-3 we get:

$$i_{1off}(0) = A - I_0 \frac{\sin(\phi)}{1-\beta^2} \tag{5-3}$$

$$i_{1on}\left(\frac{\pi}{\omega} + D\frac{\pi}{\omega}\right) = \frac{V_{in}}{L_1}\frac{\pi D}{\omega} + \gamma \tag{5-4}$$

$$i_{1off}\left(\frac{\pi}{\omega}\right) = A\cos\left(\omega_o \frac{\pi}{\omega}\right) + B\sin\left(\omega_o \frac{\pi}{\omega}\right) + I_0 \frac{\sin(\phi)}{\left(1-\beta^2\right)} \tag{5-6}$$

$$V_{in} = L_1\left[B\frac{\omega}{\beta} - I_0\cos(\phi)\frac{\omega}{\left(1-\beta^2\right)}\right] \tag{5-7}$$

where D is $\frac{\text{ton}}{\text{toff}}$ and A, B, ϕ and γ are all function of β.

Solving Eqs. 5-4 to 5-8 as a function of A, B, γ we get:

$$A - I_0 \frac{\sin(\phi)}{\left(1-\beta^2\right)} = \frac{V_{in}}{L_1}\frac{\pi D}{\omega} + \gamma \tag{5-8}$$

$$A\cos\left(\omega_o \frac{\pi}{\omega}\right) + B\sin\left(\omega_o \frac{\pi}{\omega}\right) + I_0 \frac{\sin(\phi)}{\left(1-\beta^2\right)} \tag{5-9}$$

$$V_{in} = L_1\left[B\frac{\omega}{\beta} - I_0\cos(\phi)\frac{\omega}{(1-\beta^2)}\right] \tag{5-10}$$

In order to analyze the dimming behavior of the lamp, we will normalize the above relations as follows. The current will be normalized by $\frac{Vin}{L1\omega}$, the voltages will be normalized by Vin, and all the impedance by $L1\omega$. Using this procedure, the above equations became:

$$A_n - I_0\frac{\sin(\phi)}{(1-\beta^2)} = \pi D + \gamma n \tag{5-11}$$

$$A_n\cos\left(\frac{\pi}{\beta}\right) + B_n\sin\left(\frac{\pi}{\beta}\right) + I_{on}\frac{\sin(\phi)}{(1-\beta^2)} = \gamma n \tag{5-12}$$

$$B_n = \beta + I_{on}\cos(\phi)\frac{\beta}{(1-\beta^2)} \tag{5-13}$$

Solving Eqs. 5-12 to 5-14 we get:

$$B_n = \beta + I_{on}\cos(\phi)\frac{\beta}{(1-\beta^2)} \tag{5-14}$$

$$A_n = \frac{\beta\sin\left(\frac{\pi}{\beta}\right)\left(-\beta^2+1+I_{on}\cos(\phi)\right)+\left[-\left(\pi D\beta^2\right)+\left(2I_{on}\sin(\phi)+\pi D\right)\right]}{1-\beta^2-\cos\left(\frac{\pi}{\beta}\right)+\cos\left(\frac{\pi}{\beta}\right)\beta} \tag{5-15}$$

$$\phi = -a\tan\left[\left(2\beta\sin\left(\frac{1}{\beta}\pi\right)+\pi+\pi\cos\left(\frac{1}{\beta}\pi\right)\right)\frac{\beta}{\left(\sin\left(\frac{1}{\beta}\pi\right)\pi\right)}\right] \quad (5\text{-}16)$$

$$I_{nn} = \frac{\left(\beta^3\sin\left(\frac{\pi}{\beta}\right)+\cos\left(\frac{\pi}{\beta}\right)\pi D\beta^2-\beta\sin\left(\frac{\pi}{\beta}\right)-\cos\left(\frac{\pi}{\beta}\right)\pi D\right)}{\left(\beta\sin\left(\frac{\pi}{\beta}\right)\cos(\phi)+\sin(\phi)+\cos\left(\frac{\pi}{\beta}\right)\sin(\phi)\right)} \quad (5\text{-}17)$$

Also, normalizing Eq. 3-7, we have:

$$V_{cn}(t) = -\left[\frac{-A_n}{\beta}\sin(\omega_o t)+\frac{B_n}{\beta}\cos(\omega_o t)-I_{0n}\cos(\omega t+\phi)\frac{1}{(1-\beta^2)}\right]+1 \quad (5\text{-}18)$$

Using the normalized version of Eqs. 3-6 and 3-10 , we get the input normalized current:

$$i_{1offn}(t) = \left(A_n(\beta)\cos\left(\frac{\omega}{\beta}t\right)+B_n(\beta)\sin\left(\frac{\omega}{\beta}t\right)\right)-\frac{I_{0n}\sin(\omega t+\phi(\beta))}{1-\beta^2} \quad (5\text{-}19)$$

$$i_{1on}(t) = (\omega t-\pi) \quad (5\text{-}20)$$

Where :

i1off(t) is the input current when the switch is off.

i1on(t) is the input current when the switch is off.

Assuming 100 percent efficiency, the normalized power to the lamp is equal to the normalized input power Pdcn. The normalized power is defined as the product of the normalized input current and the normalized input voltage, which is equal to one.

In order to drive the normalized power, we will integrate Eqs. 5-20 and 5-19 using the above boundary conditions.

$P_{dcn} := P_{dcon} + P_{dcoff}$

Where:

Pdcon is the normalized input power when the switch is on:

$$P_{dcon} = \frac{\omega}{\pi + D\pi}\int_0^{\frac{\pi}{\omega}}\left(A_n(\beta D)\cos\left(\frac{\omega}{\beta}t\right) + B_n(\beta D)\sin\left(\frac{\omega}{\beta}t\right)\right) - \frac{I_0 n(\beta D)\sin(\omega t + \phi(\beta D))}{1-\beta^2}dt$$

and P_{dcoffn} in the normalized input power when the switch is off:

$$P_{dcoffn} = \frac{\omega}{\pi + D\pi}\int_{\frac{\pi}{\omega}}^{(D+1)\frac{\pi}{\omega}}(\omega t - \pi)dt$$

$$P_{dcon} = \sigma\left(A_n\beta\sin\left(\frac{\pi}{\beta}\right) + \beta B_n\left(1+\cos\left(\frac{\pi}{\beta}\right)\right) + \frac{2\cos(\phi)I_0 n}{\beta^2 - 1}\right) \qquad (5\text{-}21)$$

Where :

$$\sigma = \frac{1}{\pi + D\pi}$$

$$P_{dcoffn} = \frac{5\pi D^2}{D+1} \qquad (5\text{-}22)$$

Eq. 5-23 and 5-22 give the necessary relations of the input power as a function of the D and the normalized resonant frequency β.

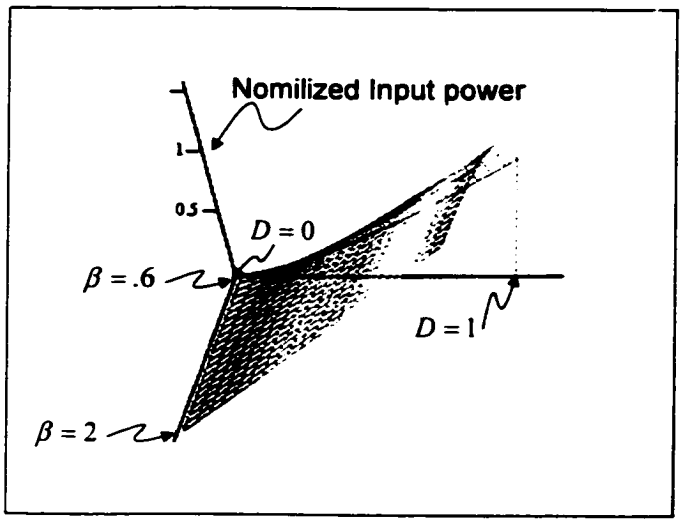

Fig. 5.2 Normalized Input Power as Function of D and β

Using a resonant frequency of 30kHz, we can see from Figure 5.2 that the best power control of the lamp is achieved for higher β. On the other hand, for $\beta < .6$, the power range decreased to almost 50 percent even for D =1 .

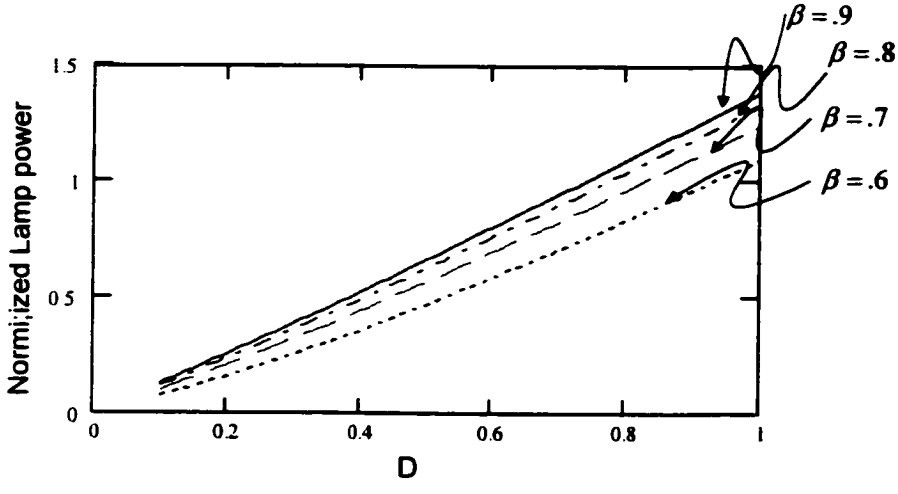

Fig. 5.3 Normalized Lamp Power as Function of D

As was shown in the above analysis, this new topology could be used as a dimmable ballast. The range is limited by the increase of the voltage across the switch. As was shown in Chapter 3, the stress on the switch increases as β is decreased.

5.3 Zero Voltage Switching Condition Verification

The main advantage of the proposed topology is its high efficiency. The fact that we only have one switch puts restriction on the dimming range while achieving zero voltage switching. In order to verify the zero voltage condition, we will need to use the generalized expression of the voltage across the switch as a function of D and β. Using Eq. 5-19, we can plot the drain to source voltage as a function of D and β.

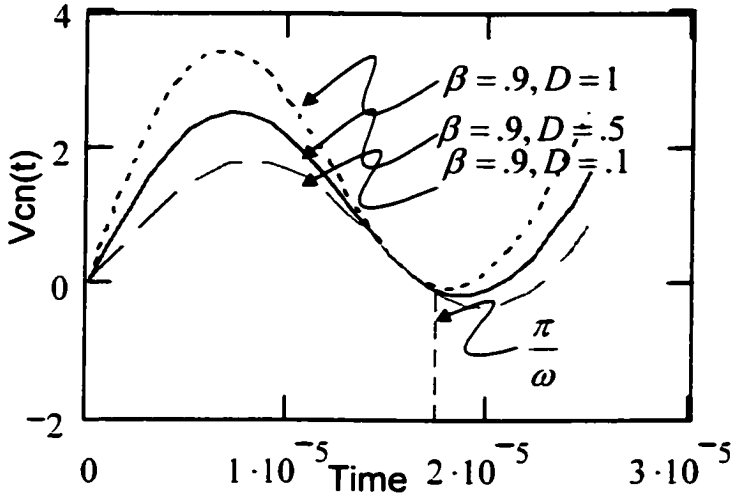

(a)

Fig. 5.4 Drain to Source Voltage as a Function of Duty Cycle D.

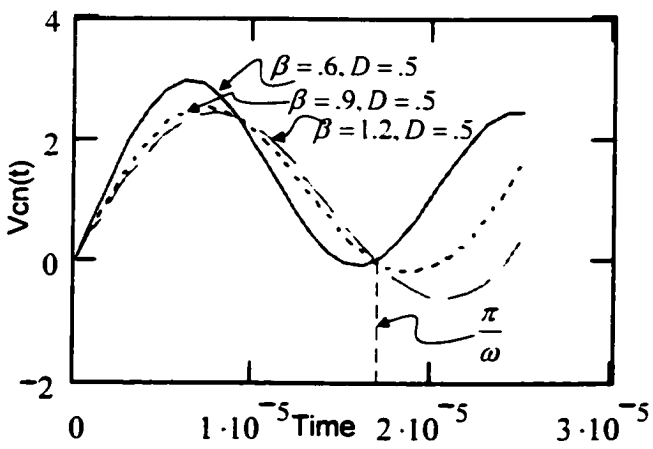

(b)

Fig. 5.4 $v_{ds}(t)$ of the Power Switch as Function of β

As can be seen from Fig. 5.4, the zero voltage switching is guaranteed for the entire range of control. We also noticed, what was already proven in Chapter 3, that the peak voltage on the switch decreases as β increases.

In this chapter, we were able to prove that using the control technique of fixed time off and variable time on, we can achieve very good dimming capability.

CHAPTER 6

CONCLUSION

As was shown in Chapter 1, electronic ballasts for gas discharge lamps received great attention in recent years due to their merits of small size, light weight, high efficacy, and long lamp life as shown in Fig. 6-1. The ballast market from 1993 to 2000 has seen a steady growth from 25 percent to 35 percent, and is expected to reach 77 percent in 2015. It is also expected to exceed a $200-million sale in 1993, and is expected to reach $1.3 billion in 2015.

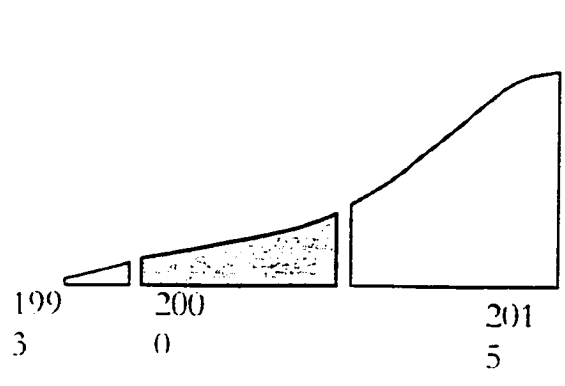

Figure 6-1 Market Ballast Evolution

The poor input PF and rich harmonic current produced if the electronic ballasts are powered directly by a simple peak rectifying circuit from the utility AC lines, necessitates the use of some current-shaping circuits before the inverter. To maintain high PF and low harmonic current, stringent regulations such as the IEC 1000-3-2 have recently been established and enforced. These regulations have stimulated considerable interest in developing cost-effective solutions in designing and manufacturing high-power-factor

electronic ballasts. A two-stage approach with a current-shaping stage (PFC stage) followed by an inverter stage is used in practical applications. However, the cost for a well-designed ballast is still high. To reduce the cost and component count, it is attractive to integrate the PFC stage with the inverter stage so that the power switch and its controller can be eliminated. The use of controllable-output electronic ballasts or dimming electronic ballasts can significantly reduce energy consumption and make intelligent lighting feasible. Recently, the development of cost-effective single-stage PFC electronic ballasts with wide-range dimming control has become a dynamic research area.

This dissertation presents a novel single-stage PF and inverter circuit correction, with wide-range dimming control techniques. The resultant issues are voltage stress in the boost-derived single-stage PFC electronic ballasts, exact modeling of the lamp, and methods to improve the crest factor and power factor.

LIST OF REFERENCES

[A1]: J. B. Murdoch, *Illumination Engineering – From Edison's Lamp to the Laser*. New York, NY: Macmillan Publishing Company, 1985, p. 5, p. 190.
[A2]: L.L. Cavalli-Sforza American 265 Nov (1991) Human Evolution
[A3]: The chemistry of artificial lighting devices. R.C. Ropp.
[A4]: "Lighting and Artificial Lighting" Encyclopedia Britannica.
[A5]: H. Schroeder, History of Electrical Light, Smithsonian Institution Publ.# 2717
[A6]: J. Fisher, Z. Tech Phys. 19- 25- 57 105.
[A7]: Illumination Engineering. Joseph B. Murdoch
[A8]: Lamp and lighting. J.R.Coaton and Marsden.
[A9]: J. Waymouth, *Electric Discharge Lamps*. Cambridge, Mass.: The M.I.T. Press.
[A10]: A. E. Emanuel and L. Peretto, "The response of fluorescent lamp with magnetic ballast to voltage distortion," IEEE Transaction on Power Delivery, Vol. 12.
[A11]: C. Meyer and H. Nienhuis, *Discharge Lamps*. Deventer, 1988.
[B1]: Michaël Bairanzade Power Semiconductor Motorola SPS Toulouse AN1543
[B2]: Michael BAIRANZADE MOTOROLA semiconductors AN 1576
[B3]: R. R. Verderber, O. C. Morse and F. Rubinstein, "Performance of Electronic Ballast and Controls with 34- and 40-Watt F40 Fluorescent Lamps," IEEE Transaction on Industry Applications, Vol. 25, No. 6, Nov./Dec. 1989, pp. 1049-1059.
[B4]: R. P. Stratford, "Harmonic pollution on power systems-a change in philosophy," IEEE Trans. on Industrial Applications, Vol. 16, no. 5, pp. 617-623, Sept./Oct. 1980.
[B5]: R. P. Stratford, "Analysis and control of harmonic current in systems with static power converters," IEEE Trans. on Industrial Applications, Vol. 17, no. 1, pp. 71-81, Jan./Feb. 1981.
[B6]: T. H. Ortmeger, etc., "The effects of power system harmonics on power system equipment and loads," IEEE Trans. on Power Apparatus and Systems. Vol. 104, no. 9, pp. 2555-2563, Sept. 1985.
[B7]: R. Redl, P. Tenti, J. D. V. Wyk, "Power electronics' polluting effects," *IEEE Spectrum*, pp. 32-39, May 1997.
[B8]: Std IEEE-519, IEEE Recommended Practice and Requirements for Harmonic Control in Electric Power Systems, 1992.
[B9]: IEC 1000-3-2, Electromagnetic Compatibility Part 3, Section 2: Limits for harmonic current emissions (equipment input current ≤ 16A per phase), March 1995.
[B10]: T. S. Key, J. S. Lai, "IEEE and international harmonic standards impact on power electronics equipment design," *IEEE IECON record*, pp. 430-436, 1998.
[B11]: G. H. Robinson, "Harmonic phenomena associated with the Benmore-Harwards HVDC transmission scheme," *New Zealand Engineering*, pp. 16-29, Jan. 1966.
[B12]: E. W. Kimbark, Direct Current Transmission, *John-Wiley & Sons, Inc.*, New York, 1971.

[B13]: R. P. Stratford, "Rectifier harmonics in power systems," *IEEE Trans. on Industrial Applications*, Vol. 16, no. 3, pp. 271-276, Mar./Apr. 1980.
[B14]: R. P. Stratford, "Harmonic pollution on power systems-a change in philosophy," *IEEE Trans. on Industrial Applications*, Vol. 16, no. 5, pp. 617-623, Sept./Oct. 1980.
[B15]: R. Redl, P. Tenti, J. D. V. Wyk, "Power electronics' polluting effects," *IEEE Spectrum*, pp. 32-39, May 1997.
[B16]: R. P. Stratford, "Analysis and control of harmonic current in systems with static power converters," *IEEE Trans. on Industrial Applications*, Vol. 17, no. 1, pp. 71-81, Jan./Feb. 1981.
[B17]: T. H. Ortmeger, etc., "The effects of power system harmonics on power system equipment and loads," *IEEE Trans. on Power Apparatus and Systems*. Vol. 104, no. 9, pp. 2555-2563, Sept. 1985.
[B18]: J. Qian and F. C. Y. Lee, "A high-efficiency single-stage single-switch high-power-factor AC/DC converter with universal input," *IEEE Trans.Power Electron.*, Vol. 13, pp. 699–705, July 1998.
[B19]: Huai Wei; Batarseh, I., "Comparison of basic converter topologies for power factor correction" *Southeastcon '98. Proceedings. IEEE* , 1998 Page(s): 348 -353
[B20]: F.-S. Tsai, P. Markowski, and E. Whitcomb, "Off-line flyback converter with input harmonic current correction," *in Proc. INTELEC'96*, 1996, pp. 120–124.
[B21]: J. Qian, Q. Zhao, and F. C. Lee, "Single-stage single-switch power-factor-correction AC/DC converters with DC-bus voltage feedback for universal line applications," *IEEE Trans. Power Electron*, Vol. 13, pp.1079–1088, Nov. 1998.
[B22]: I. Takahashi, "Power factor improvement of a diode rectifier circuit by dither signals," Conference Record of IEEE-IAS 1990, pp. 1289-1294.
[B23]: W. L. Eaton and A. B. Murray, "Reduction of Harmonics in Gas Discharge Lamp Ballasts," US Patent No. 4,511,823, April 16, 1985.
[B24]: J. J. Spangler, "A Power Factor Corrected, MOSFET, Multiple Output, Flyback Switching Supply," PCI Proceedings, Oct. 1985, pp. 19-32.
[B25]: M. H. Kheraluwala, R. L. Steigerwald and R. Gurumoorthy, "A Fast-Response High Power Factor Converter with a Single Power Stage," Conference Record of IEEE-PESC 1991, pp. 769-779.
[B26]: M. T. Madigan, R. W. Erickson and E. H. Ismail, "Integrated High-Quality Rectifier-Regulators," IEEE Transactions on Industrial Electronics, Vol. 46 No. 4, Aug. 1999 pp. 749 – 758.
[B27]: S. Teramoto, M. Sekine and R. Satio, "High Power Factor AC/DC Converter," US Patent No. 5,301,095, April 5, 1994.
[B28]: Y. Jiang and F. C. Lee, "Single-stage single-phase parallel power factor correction scheme," Conference Record of IEEE-PESC 1994, pp. 1145-1151.
[B29]: R. Redl, L. Balogh and N. O. Sokal, "A New Family of Single-Stage Isolated Power-Factor Correctors with Fast Regulation of the Output Voltage," Conference Record of IEEE-PESC 1994, pp. 1137-1144.

[B30]: H. Watanabe, Y. Kobayashi, Y. Sekine, M. Morikawa and T. Ishii, "The suppressing harmonic currents, MS (magnetic-switch) power supply," Conference Record of IEEE-INTELEC 1995, pp. 783-790.
[B31]: J. Zhang, L. Huber, M. M. Jovanovic and F. C. Lee, "Single-Stage Input-Current-Shaping Technique with Voltage-Doubler-Rectifier Front End," IEEE Transactions on Power Electronics, Vol. 16 No.1, Jan. 2001, pp. 55-63.
[B32]: F. S. Tsai, P. Markowski and E. Whitcomb, "Off-Line Flyback Converter with Input Harmonic Current Correction," Conference Record of IEEE-INTELEC 1996, pp. 120-124.
[B33]: J. Qian, Q. Zhao and F. C. Lee, "Single-Stage Single-Switch Power-Factor-Correction AC/DC Converters with DC-Bus Voltage Feedback for Universal Line Applications," IEEE Transactions on Power Electronics, Vol. 13 No. 6, Nov. 1998, pp. 1079-1088.
[B34]: L. Huber and M. M. Jovanovic, "Design Optimization of Single-Stage, Single-Switch Input-Current Shapers," Conference Record of IEEE-PESC 1997, pp. 519-526.
[B35]: G. Hua, "Consolidated Soft-Switching AC/DC Converters," US Patent No. 5,790,389, Aug. 4, 1998.
[B36]: Weihong Qiu; Wenkai Wu; Shiguo Luo; Wei Gu; Batarseh, I. Applied Power Electronics Conference and Exposition, 2002. APEC 2002. Seventeenth Reference 166
[B37]: J. Rozenboom, "The Electronic Ballast Circuit and Low Pressure Lamps," Int. Journal Electronics, Vol. 82, No. 3, 1997, pp. 269-294.
[B38]: J. Ribas, J. M. Alonso, E. L. Corominas, A. J. Calleja and M. Rico-Secades, "Design Considerations for Optimum Ignition and Dimming of Fluorescent Lamps Using a Resonant Inverter Operating Open Loop," Conference Record of IEEE-IAS 1998, pp. 2068-2075.
[B39]: C. S. Moo, H. L. Chung, H. N. Chen and H. C. Yen, "Design Dimmable Electronic Ballast with Frequency Control," Conference Record of IEEE-APEC 1999, pp. 727-733.
[B40]: T. F. Wu, T. H. Yu and M. C. Chiang, "Single-Stage Electronic Ballast with Dimming Feature and Unity Power Factor," IEEE Transactions on Power Electronics, Vol. 13, No. 3, May 1998, pp. 586-597.
[B41]: T. F. Wu and T. H. Yu, "Analysis and Design of a High Power Factor, Single-Stage Electronic Dimming Ballast," IEEE Transactions on Industry Applications,Vol. 34, No. 3 May/June 1998, pp. 606-615.
[B42]: C. Branas, F. J. Azcondo and S. Bracho, "Electronic Ballast for HPS Lamps with Dimming Control by Variation of the Switching Frequency: Soft Start-up Method for HPS and Fluorescent Lamps," Conference Record of IEEE-IECON 1998, pp. 953-958.
[B43]: T. J. Ribarich and J. J. Ribarich, "A New Control Method for Dimmable High-Frequency Electronic Ballasts," Conference Record of IEEE-IAS 1998, pp. 2038-2043.
[B44]: J. H. Reijnaerts, "Circuit Arrangement for Reducing Striations in a Low-Pressure Mercury Discharge Lamp," US Patent No. 5,369,339, Nov. 29, 1994.
[B45]: R. L. Steigerward and L. D. Stevanovic, "Elimination of Striations in Fluorescent Lamps Driven by High-Frequency Ballasts," US Patent No. 5,701,059, Dec. 23,1997.

[B46]: C. R. Sullivan, "Control System for Proving Power to A Gas Charge Lamp," US Patent No. 5,864,212, Jan. 26, 1999.
[B47]: C. Branas, F. J. Azcondo and S. Bracho, "Fluorescent Lamps: Introduction to Quasi-Optimum Control," Conference Record of IEEE-IAS 1998, pp. 970-975.
[B48]: T. F. Wu, Y. C. Liu and Y. J. Wu, "High-Efficiency Low-Stress Electronic Dimming Ballast for Multiple Fluorescent Lamps," IEEE Transactions on Power Electronics, Vol. 14, No. 1, Jan. 1999, pp. 160-167.
[C1]: A.K. Bhat and S. B. Dewan ' Analysis and design of high frequency resonant converter using LCC-type commutation ' IEEE 1986 PP 657-663.
[C2]: A.K. Bhat and S. B. Dewan 'Steady state analysis of LCC-type commutated high frequency inverter' IEEE Power Electronics 1988 pp. 1220-1227
[C3]: R.L.Steigerwald, ' A comparison of half-bridge resonant converter topologies' IEEE Power Electronics 1988 pp.174-182
[C4]: I. Batarseh, R. Liu and C.Q. Lee 'Design of parallel resonant converter with LCC-type commutation' Electronics letter, Vol. 24 pp. 177-179
[C5]: I. Batarseh, R. Liu and C.Q. Lee and A.K. Upadhyay. '150 watt and 140 kHz multi-output LCC-Type parallel resonant converter 'IEEE APEC 1989 pp. 221-230
[C6]: I. Batarseh and C.Q. Lee 'High–frequency high order parallel resonant converter IEEE Vol. IE-36 1989 pp. 485-492
[C7]: Zaki Moussaoui and I. Batarseh 'Performance characteristic of the series Parallel resonant converter' Southcon/94. Conference Record , 1994 Page(s): 573 -577
[C8]: N. O. Sokal and A. D. Sokal, "Class E—a new class of high-efficiency tuned single-ended switching power amplifiers," IEEE J. Solid-State Circuits, Vol. 10, pp. 168–176, June 1975.
[C9]: "High-efficiency tuned switching power amplifier," U. S. Patent 3 919 656, Nov. 1975.
[C10]: F. H. Raab, "Idealized operation of the class E tuned power amplifier," IEEE Trans. Circuits Syst., Vol. 24, pp. 725–735, Dec. 1977.
[C11]: M. K. Kazimierczuk and K. Puczko, "Exact analysis of class-E tuned power-amplifier at any q and switch duty cycle," IEEE Trans. Circuits Syst., Vol. CAS-34, pp. 149–159, Feb. 1987.
[C12]: C. P. Avratoglou and N. C. Voulgaris, "A new method for the analysis and design of the class-E power- amplifier taking into account the q(l) factor," IEEE Trans. Circuits Syst., Vol. CAS-34, pp. 687–691, June 1987.
[C13]: C.-H. Li and Y.-O. Yam, "Maximum frequency and optimum performance of class-E power-amplifiers," Proc. Inst. Electr. Eng. Circuits Devices Syst., Vol. 141, pp. 174–184, June 1994.
[C14]: J. C. Mandojana, K. J. Herman, and R. E. Zulinski, "A discrete continuous time-domain analysis of a generalized class-E amplifier," IEEE Trans. Circuits Syst., Vol. 37, pp. 1057–1060, Aug. 1990.
[C15]: C. P. Avratoglou, N. C. Voulgaris, and F. I. Ioannidou, "Analysis and design of a generalized class-E tuned power-amplifier," IEEE Trans. Circuits Syst., Vol. 36, pp. 1068–1079, Aug. 1989.

[C16]: W. H. Press, S. A. Teukolsky, W. T. Vetterling, and B. P. Flannery, Numerical Recipes in C: The Art of Scientific Computing. Cambridge, U.K.: Cambridge Univ. Press, 1992, pp. 742–743.
[C17]: M. K. Kazimierczuk and K. Puczko, "Power-output capability of class-E amplifier at any loaded-Q and switch duty cycle," IEEE Trans. Circuits Syst., Vol. 36, pp. 1142–1143, Aug. 1989.
[C18]: "Class E tuned power amplifier with anti-parallel diode or series diode at switch, with any loaded Q and switch duty cycle," IEEE Trans. Circuits Syst., Vol. 36, pp. 1201–1209, Sept. 1989.
[D1]: T. H. Yu, H. M. Huang, and T. F. Wu, "Self-excited half-bridge series resonant parallel loaded fluorescent lamp electronic ballasts," in IEEE APEC Conf. Rec., 1995, pp. 657–664.
[D2]: Y. Sun, "Using PSpice to determine lamp current variations due to electronic ballast component tolerance," in IEEE Industry Applications Soc. Conf. Rec., 1994, pp. 1974–1978.